HHS Public Access

Author manuscript

Cell Rep. Author manuscript; available in PMC 2022 November 15.

Published in final edited form as:

Cell Rep. 2022 April 12; 39(2): 110575. doi:10.1016/j.celrep.2022.110575.

Brown adipose tissue involution associated with progressive restriction in progenitor competence

Zan Huang[1,2,3,12,*], **Zengdi Zhang**[3,12], **Zahra Moazzami**[3], **Ryan Heck**[3], **Ping Hu**[4], **Hezkiel Nanda**[5], **Kaiqun Ren**[3,6], **Zequn Sun**[7], **Alessandro Bartolomucci**[3], **Yan Gao**[8], **Dongjun Chung**[9], **Weiyun Zhu**[1,2], **Steven Shen**[5,10], **Hai-Bin Ruan**[3,11,13,*]

[1]Laboratory of Gastrointestinal Microbiology, Jiangsu Key Laboratory of Gastrointestinal Nutrition and Animal Health, College of Animal Science and Technology, Nanjing Agricultural University, Nanjing, Jiangsu 210095, China

[2]National Center for International Research on Animal Gut Nutrition, Nanjing Agricultural University, Nanjing, Jiangsu 210095, China

[3]Department of Integrative Biology and Physiology, University of Minnesota Medical School, Minneapolis, MN 55455, USA

[4]Department of Prenatal Diagnosis, Women's Hospital of Nanjing Medical University, Nanjing Maternity and Child Health Care Hospital, Nanjing, Jiangsu 210004, China

[5]Institute for Health Informatics, University of Minnesota Medical School, Minneapolis, MN 55455, USA

[6]College of Medicine, Hunan Normal University, Changsha, Hunan 410081, China

[7]Department of Public Health Sciences, Medical University of South Carolina, Charleston, SC 29425, USA

[8]Department of Human Anatomy, School of Basic Medical Sciences, Capital Medical University, Beijing 100069, China

[9]Department of Biomedical Informatics, The Ohio State University, Columbus, OH 43210, USA

[10]Clinical Translational Science Institute, University of Minnesota Medical School, Minneapolis, MN 55455, USA

[11]Center for Immunology, University of Minnesota Medical School, Minneapolis, MN 55455, USA

[*]Correspondence: hruan@umn.edu (H.-B.R.), huangzan@njau.edu.cn (Z.H.).

AUTHOR CONTRIBUTIONS

Z.H. and Z.Z. designed and performed experiments, analyzed data, and wrote the manuscript. Z.M. performed Seahorse experiments. R.H. and K.R. assisted with mouse colony management and experiments. P.H. collected human fetal iBAT. Z.S. and D.C. performed longitudinal transcriptomics analyses of bulk RNA-seq of SVF cells. A.B. helped with metabolic phenotyping. Y.G. helped with generation of *Fstl1* KO mice. W.Z. supported Z.H. in obtaining funding. H.N. and S.S. analyzed rabbit scRNA-seq data. H.-B.R. conceived the project, designed experiments, analyzed data, and wrote the manuscript.

SUPPLEMENTAL INFORMATION

Supplemental information can be found online at https://doi.org/10.1016/j.celrep.2022.110575.

DECLARATION OF INTERESTS

The authors declare no competing interests.

[12]These authors contributed equally

[13]Lead contact

SUMMARY

Human brown adipose tissue (BAT) undergoes progressive involution. This involution process is not recapitulated in rodents, and the underlying mechanisms are poorly understood. Here we show that the interscapular BAT (iBAT) of rabbits whitens rapidly during early adulthood. The transcriptomic remodeling and identity switch of mature adipocytes are accompanied by loss of brown adipogenic competence of progenitors. Single-cell RNA sequencing reveals that rabbit and human iBAT progenitors highly express the *FSTL1* gene. When iBAT involutes in rabbits, adipocyte progenitors reduce *FSTL1* expression and are refractory to brown adipogenic recruitment. Conversely, FSTL1 is constitutively expressed in mouse iBAT to sustain WNT signaling and prevent involution. Progenitor incompetence and iBAT paucity can be induced in mice by genetic deletion of the *Fstl1* gene or ablation of *Fstl1*$^{+}$ progenitors. Our results highlight the hierarchy and dynamics of the BAT progenitor compartment and implicate the functional incompetence of FSTL1-expressing progenitors in BAT involution.

Graphical abstract

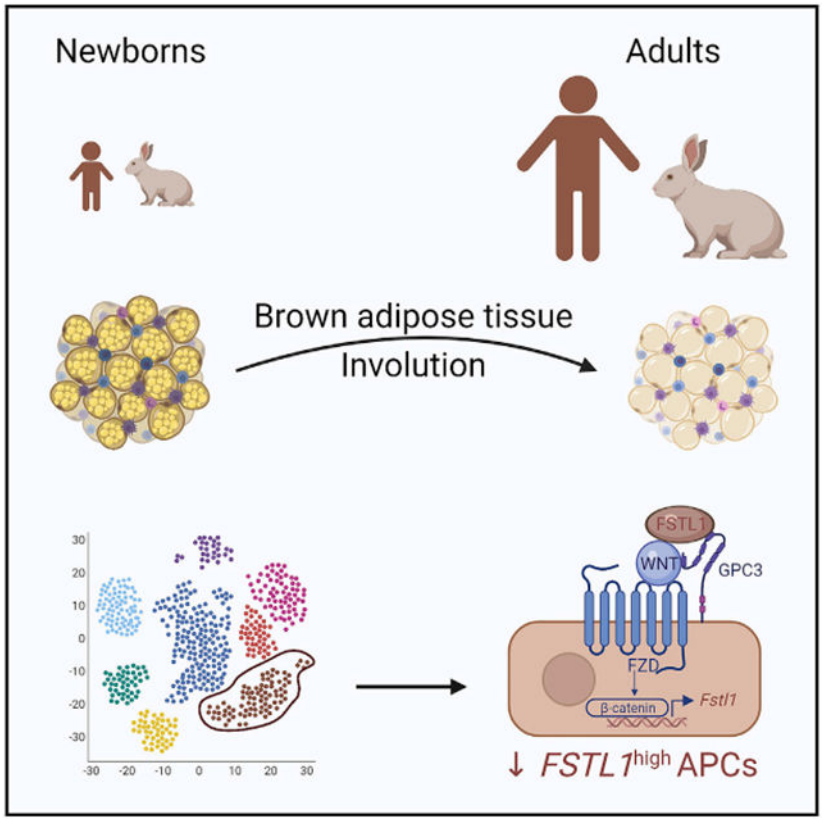

In brief

One challenge for targeting brown adipose tissue (BAT) to combat metabolic diseases is a lack of knowledge of the regulation of age-dependent BAT involution in humans. Using rabbits as a model, Huang et al. propose that the functional restriction of FSTL1-expressing adipocyte progenitors contributes to BAT involution.

INTRODUCTION

Obesity is a strong predisposing factor for many diseases, including hypertension, high cholesterol, diabetes, and cardiovascular diseases. The thermogenic brown adipose tissue (BAT) not only dissipates chemical energy as heat to maintain body temperature and energy balance (Cannon and Nedergaard, 2004; Rosen and Spiegelman, 2014; Yang and Ruan, 2015) but also serves as a metabolic sink for glucose, fatty acids, and branched-chain amino acids to improve metabolic health (Maurer et al., 2019; Yoneshiro et al., 2019; Li et al., 2021). Therefore, BAT has been increasingly acknowledged as a potential therapeutic target for obesity and related disorders (Wang et al., 2020).

Two spatiotemporally distinct phases of BAT ontogeny have been indicated in humans. BAT first appears mainly in interscapular and perirenal regions during mid-gestation (Lidell, 2019). Although maximally recruited in neonates, interscapular BAT (iBAT) rapidly atrophies until it is barely detectable in adults (Heaton, 1972; Sidossis and Kajimura, 2015). Perirenal BAT also steadily transforms to white adipose tissue (WAT) with increasing age (Tanuma et al., 1975). The second developmental phase occurs postnatally and gives rise to anatomically dispersed BAT in cervical, supraclavicular, and axillary areas in adult humans (Rogers, 2015; Ruan, 2020). The prevalence of cervical-supraclavicular BAT peaks in adolescence and then reduces to less than 5% in middle-aged subjects (Rogers, 2015). Cold recruits BAT, even in subjects having no existing metabolically active BAT (Saito et al., 2009; van Marken Lichtenbelt and Schrauwen, 2011; Yoneshiro et al., 2011). Such recruitment reportedly happens mostly in young adults, and there is limited evidence that BAT can be efficiently recruited in middle-aged and aged people (Hanssen et al., 2015). We define this age-related decline in the number and function of parenchymal brown adipocytes (not the shrinkage of tissue mass) as BAT involution; however, the cellular and molecular mechanisms governing the involution process remain enigmatic.

Compared with that in humans, there is limited involution or atrophy of BAT associated with life history in mice housed at standard room temperature. iBAT adipocytes remain as the progeny of *Myf5*$^{+}$ cells (Sanchez-Gurmaches and Guertin, 2014) and can be immediately recruited by external cues, such as cold and sympathetic activation in old mice, although to a slightly lesser extent (Sellayah and Sikder, 2014; Goncalves et al., 2017; Tajima et al., 2019). Under thermoneutral conditions and in mice fed an energy-rich diet, iBAT still retains its browning capacity and can be recruited to full functionality (Cui et al., 2016; Razzoli et al., 2016; Roh et al., 2018; de Jong et al., 2019). These observations not only indicate that mice are inadequate for modeling the involution process of human iBAT but also suggest that non-environmental mechanisms exist to control the divergent aging program of iBAT across species.

In eutherian mammals, thermogenic capacity is negatively correlated with body mass (Loncar, 1991; Oelkrug et al., 2015). The mouse, a small animal, relies heavily on BAT to cope with its unfavorable body surface-to-volume ratio. Compared with mice, rats possess relatively more evident age-dependent iBAT remodeling that is characterized by tissue hypertrophy and whitening, reduced expression of uncoupling protein 1 (UCP1), and thermogenic dysfunction (Horan et al., 1988; McDonald et al., 1988; Florez-Duquet et al., 1998). However, iBAT involution in rats is still far less and slower than in humans. Here we use the larger rabbits to investigate the involution process of iBAT. Rabbit iBAT irreversibly transforms to WAT before puberty, at a similar developmental stage when human iBAT mostly disappears. Adipocyte precursors in iBAT of rabbits reprogram the transcriptome and lose their competence to be differentiated into mature brown adipocytes. Single-cell RNA sequencing (scRNA-seq) of stromal vascular fraction (SVF) cells identifies comparable *FSTL1*^{high} cells as potential brown adipocyte progenitors in neonatal rabbits and fetal humans. The constitutive presence of iBAT in mice is associated with high-level expression of FSTL1 in adipocyte progenitors. Genetic deletion of FSTL1 in brown adipocyte progenitors causes progenitor incompetence and iBAT paucity in mice. Preserving or regenerating *FSTL1*^{high} brown adipocyte progenitors may provide an avenue to prevent BAT involution or rejuvenate aged BAT, promoting metabolic fitness.

RESULTS

Progressive BAT whitening in young rabbits

To characterize BAT involution in rabbits, we collected interscapular, subscapular, and suprascapular fat depots from New Zealand White rabbits at the ages of 1 day and 3, 6, and 12 weeks (Figure S1A). All depots had the typical morphology of BAT in neonatal rabbits (Figure 1A). Tissue whitening, adipocyte hypertrophy, and loss of UCP1 expression could be readily seen starting at 3 weeks of age and full conversion to WAT-like tissues at 12 weeks (Figures 1A and 1B). To verify the morphological observations, we performed RNA-seq of total iBAT. Principal-component analysis showed a clear separation of iBAT from neonatal and 3-week-old rabbits, whereas 6- and 12-week samples were clustered together (Figure 1C). The majority of changes in gene expression happened at 3 weeks, and there were much fewer differentially expressed genes at 6 and 12 weeks (Figure S1B). Hierarchical clustering and pathway analysis showed that early differentially expressed genes were involved in processes including angiogenesis, the tricarboxylic acid cycle, skeletal muscle development, mitochondrial electron transport, and brown fat differentiation and thermogenesis (Figure S1C), which are all associated with BAT function. On the other hand, late-changing genes control metabolic processes like ATP synthesis, fatty acid oxidation and biosynthesis, and glucose metabolism, representing metabolic adaptation to tissue whitening. We did not observe enrichment of any cell death pathways. No evident apoptosis, based on cleaved caspase-3 expression (Figure S1D), was detected, suggesting that rabbit iBAT involution is mainly driven by transformation of adipocyte fate rather than cell death.

Were those unilocular and UCP1-negative adipocytes found in regressed rabbit iBAT white adipocytes or “dormant,” inactive brown adipocytes? Brown adipocyte markers, including

UCP1, DIO2, and *PPARGC1A*, were dramatically downregulated from day 1 to week 12 in rabbit iBAT (Figure 1D). The levels of beige markers, including *TBX1* and *CD137*, were relatively stable (Roh et al., 2018), whereas expression of white markers gradually increased over time (Figure 1D). Sympathetic nerve activity dictates BAT lipolysis and thermogenesis, and we found a substantial reduction in the expression of β1-3 (*ADRB1-3*) and α1A and α1B (*ADRA1A* and *ADRA1B*, respectively) adrenergic receptors (ARs) and upregulation of α1D (*ADRA1D*) and α2 (*ADRA2A* and *ADRA2B*) receptors in rabbit iBAT (Figures 1E and S1E). However, the expression of tyrosine hydroxylase (TH; a marker of sympathetic neurons) was surprisingly increased over the course of iBAT involution (Figure 1F). This points to possible intrinsic causes of the alterations in AR expression and suggests that BAT involution in rabbits is unlikely to be a result of dysfunctional sympathetic tone. A handful of studies in mice have demonstrated that sympathetic suppression by warming (Roh et al., 2018), βAR knockout (Razzoli et al., 2016), or neurotrophic defect (Zeng et al., 2019) is not sufficient to convert BAT to a WAT identity.

To determine whether whitened iBAT can be remodeled by cold, we compared adult rabbits obtained from a non-climate-controlled rabbitry in Wisconsin during summer (August 2017 with an average temperature of 21°C) or early spring (March 2018 with an average temperature of 0°C). A cold environment did not prevent whitening and loss of UCP1 in adult iBAT (Figures 1G and 1H). These results, together with the β3AR agonism experiment, indicate a WAT-like identity of rabbit interscapular fat during adulthood.

Restriction of progenitor competence during iBAT involution

In addition to transformation of mature adipocytes, we went on to determine whether iBAT involution in rabbits is associated with impaired browning capacity of adipocyte progenitor cells. The SVF cells from iBAT of neonatal rabbits could be differentiated *in vitro* into *UCP1*-expressing adipocytes using a “brown” adipogenic cocktail (Figures 1I and 1J; Cambon et al., 1998). As rabbits grew, although no changes in cell proliferation were observed (Figure S2A), SVF cells from 3- to 12-week-old rabbits displayed slightly reduced adipogenic differentiation, as shown by less lipid deposition (Figure 1I) and lower expression levels of the *ADIPOQ, FABP4*, and *PLIN2* genes (Figure S2B). The expression of thermogenic *UCP1* (about 1,000-fold lower at 3 weeks and not detectable [Cycle threshold values >40] at 6 and 12 weeks) and *DIO2* was downregulated more drastically, either normalized to the housekeeping gene *RPLP0* (Figures S2C and S2D) or normalized to the geometric mean of the *ADIPOQ, FABP4*, and *PLIN2* genes (Figure 1J). Conversely, expression of the white adipocyte-enriched *LEP* gene was positively correlated with rabbit age (Figure 1J). As a result, adipocytes differentiated from 12-week SVF cells had a reduced oxygen consumption rate and uncoupling respiration (Figure S2E). On the other hand, when inducing differentiation using a “white” adipogenic cocktail, 12-week SVF cells demonstrated much greater potential to become adipocytes compared with neonatal SVF cells (Figure S2F). These data suggest that the age-dependent decline of SVF cells in thermogenic differentiation was not merely a result of defective adipogenic potential but, rather, their fate switching.

To further determine the brown adipogenic potential of progenitors *in vivo*, we implanted rabbit SVF cells from iBAT and subscapular BAT (sBAT) into the dorsal region of immunodeficient mice (Min et al., 2016; Figure 1K). SVF cells from neonatal rabbits could form largely multilocular and UCP1-positive brown adipocytes (Figure 1L). However, in implants derived from older SVF cells, unilocular and UCP1-low/negative adipocytes gradually emerged and finally dominated. Correlated with the reduced competence to be differentiated into brown adipocytes, there was transcriptional reprograming in SVF cells from rabbit iBAT and sBAT (Figures S2G and S2H). RNA-seq of SVF cells revealed a large number of differentially expressed genes from day 1 to 3 weeks of age (Figures S2H and S2I). A second wave of transcriptional change was observed at week 12 (Figures S2I and S2J), possibly indicative of adaptive responses to tissue whitening. To profile early molecular changes in adipocyte progenitors, we excluded the 12-week data point and subjected SVF transcriptomes to longitudinal analyses. Differentially expressed genes in iBAT and sBAT SVF cells were merged and clustered into six groups. Clusters 1–3 showed downregulation with distinct patterns: continued downregulation, early downregulation, and late downregulation (Figure S2K). Clusters 4–6 represented genes that had continued upregulation, early upregulation, and late upregulation, respectively (Figure S2L). Pathway analysis showed that downregulated genes were enriched for muscle contraction and mitochondrial function, whereas upregulated genes were involved in translation and metabolism of lipids and amino acids (Figure S2M). These data demonstrate that periscapular BAT involution in rabbits is associated with functional incompetence and transcriptional reprogramming of adipocyte progenitors.

Dynamic transcriptional landscape of the SVF of rabbit BAT at the single-cell level

To understand the developmental heterogeneity and dynamics of BAT stromal cells, we then performed scRNA-seq of freshly isolated iBAT SVF cells from rabbits at the age of 1 day, 3 weeks, and 12 weeks. A total of 9,799 cells (1,542, 6,305, and 1,592 cells from day 1, 3-week, and 12-week rabbits, respectively) were analyzed (Table S1). Unsupervised clustering of the gene expression profiles identified 9 cell populations (Figures 2A and S3A; Table S2). Group 2, 0, and 3 cells were adipose progenitors because they predominantly expressed canonical adipose mesenchymal markers, including *WNT2, DLK1*, and *THY1* (*CD90*) (Figure 2B). Adipocyte identity genes, including *FABP4, LPL, PPARG*, and *APOD*, were specifically enriched in group 1 and 4 cells (Figures 2C and S3B), indicating that these cells were “committed preadipocytes.” Previously identified mesenchymal markers in mice and humans, such as *PDGFRA, PDGFRB*, and *CD34*, were expressed by progenitor and preadipocyte populations (Figure S3B). By searching for marker genes that encode cell surface proteins, we identified *SFRP4* as a marker for progenitors (Figure 2B) and *VCAM1* (*CD106*) and *NRP1* (*CD304*) as preadipocyte markers (Figure 2C), which were used later for flow cytometry analyses of these populations in mice.

SVF cells from rabbits at different ages were readily separated at the single-cell level (Figure 2D). The majority of day 1 SVF cells were group 2 progenitors (84.0%) and group 6 cycling cells (7.6%) marked by genes involved in cell cycle control, such as *MKI67, CENPF*, and *PCNA* (Figures 2D and S3B; Table S1). Non-hematopoietic SVF cells in 3-week-old rabbits were largely composed of group 0 and 3 progenitors (35.9% and 11.1%,

respectively) and group 1 committed preadipocytes (33.8%). At 12 weeks of age, group 3 progenitors (29.8%) and group 4 committed preadipocytes (51.0%) were dominant. After normalizing to cell number, we could observe a gradual transition of progenitors from group 2 to group 0 and then to group 3 as rabbits grew older (Figure 2E; Table S1). Very few committed preadipocytes (i.e., groups 1 and 4) were found in neonatal rabbits. There were fewer and fewer group 6 cycling cells as rabbits grew up, indicating precursor cells transitioning from self-renewal to differentiation.

iBAT-resident progenitors in older rabbits gradually lost their brown adipogenic competence and shifted their transcriptomic landscape. Group 2 cells (95.5% from day 1 rabbits) shared many marker genes with the *Pdgfra*$^+$ brown adipocyte progenitors identified in mouse iBAT (Figure S3C; Shamsi et al., 2021). We listed positively and negatively enriched genes of group 2 cells and performed pathway analysis (Table S3). Top activated pathways included EIF2 and the mammalian target of rapamycin (mTOR) signaling (Figure S3D), consistent with previous findings that mTOR and protein translation are essential for BAT development and thermogenesis (Ye et al., 2019). In comparison, group 0 and 3 cells were enriched with distinct sets of genes (Figure S3E). These data show that involution of rabbit iBAT changes the transcriptional and cellular landscape of the adipose precursor compartment.

Identification of conserved markers for human and rabbit brown adipose progenitors

iBAT in rabbits and humans undergoes rapid involution in early life. An important question is whether analogous populations of adipocyte progenitors exist in rabbits and humans. To address this, we isolated SVF cells from iBAT of a human fetus at the gestational age of 24 weeks after an induced abortion and subjected them to scRNA-seq analysis. The identity of collected iBAT was confirmed by H&E and UCP1 immunostaining (Figures S4A and S4B). We identified four groups (0, 1, 3, and 2) of *PDGFRα*$^+$ adipogenic lineage cells as well as pericytes, endothelial cells, lymphatic endothelial cells, hematopoietic/immune cells, and actively cycling cells (Figures 3A, S4C, and S4D; Table S4). Group 0 cells were brown adipocyte progenitors highly expressing mesenchymal marker genes, including *DLK1, THY1*, and *CD34* (Figures 3B and S4D). Group 1 and 3 cells gradually ceased expression of these mesenchymal markers and began to express genes such as *FABP4, LPL, PPARG, IGFBP5, APOE*, and *PLIN2* (Figures 3B, 3C, and S4D), indicating that they were precursor cells undergoing adipogenic differentiation. The expression of these genes was highest in group 2 committed brown preadipocytes (Figures 3C and S4D).The transcriptional hierarchy of adipogenic stromal cells supports previous histology findings showing that human iBAT is actively growing and differentiating at this gestational stage (Merklin, 1974).

We then profiled the expression of newly identified white adipocyte progenitor marker genes (Rondini and Granneman, 2020) in human BAT stromal cells. *PI16* was also expressed by group 0 cells, appearing as a common marker for brown and white adipocyte progenitors (Figure S4E). However, *DPP4, F3* (*CD142*), *CD55, EBF2* (Wang et al., 2014), and *ANAX3* were barely expressed and not enriched in any stromal population of cells (Figure S4E), suggesting that brown and white adipocyte progenitors have distinct transcriptional profiling, a result of their different developmental origins (Sanchez-Gurmaches et al., 2016).

To evaluate the analogy between human and rabbit brown adipocyte progenitors, we compared positive marker genes of human group 0 progenitors and rabbit group 2 progenitors and were able to identify 50 overlapping genes (Figure 3D; Table S5). Among them, 9 markers had log2-fold change values greater than 0.5 (Figure 3D; Table S6). These genes are *DLK1* (Figures 2B and 3B), *FSTL1*, *CILP, GPC3, COL12A1, MFAP4, FBN1, POSTN*, and *FBLN5* (Figure 3E). Interestingly, 19 of the 50 overlapping genes encode extracellular proteins (Table S5). All top 9 shared marker genes encode peptides that can be released or extracellular matrix proteins, indicating the high secretory activity of brown adipocyte progenitors. Hereafter, we refer to them as *FSTL1*^{high} cells.

To determine the expression trajectory of *FSTL1*^{high} progenitor marker genes, we performed pseudotime analysis of human and rabbit iBAT stromal cells (Cao et al., 2019). As expected, expression of the *FABP4* and *LPL* genes increased, whereas mesenchymal genes such as *THY1* and *DLK1* decreased along the adipogenic differentiation trajectory. The majority of the shared marker genes for brown adipocyte progenitors, including *FSTL1*, were consistently downregulated as human and rabbit cells left the progenitor compartment (Figures 3F and 3G).

Involuted iBAT progenitors have limited brown adipogenic competency upon β3-AR activation

We sought to determine the transcriptional dynamics of brown adipocyte progenitors. All 9 of the aforementioned common markers for brown adipocyte progenitors, *FSTL1* included, reduced their expression as rabbits grew older (Figure 4A; Table S7). Hereafter, we denote adipocyte progenitors within the involuted iBAT as *FSTL1*^{intermediate} cells. A group of genes (*DNAH1*, *CCDC93, SULF2, TMPRSS4*, and *HK3*) was upregulated in *FSTL1*^{intermediate} progenitors during involution (Table S7). These late-onset genes were largely not expressed by *FSTL1*^{high} brown progenitors from human fetal iBAT (Figure S5A). Conversely, WAT progenitor markers, including *DPP4* and *PI16*, started to express in *FSTL1*^{intermediate} progenitors (Figure S5B), indicating that *FSTL1*^{intermediate} cells in involuted iBAT became, or at least gained transcriptional properties of, white adipocyte progenitors.

It has been shown in mice that β3-AR activation stimulates beige adipogenesis (Jiang et al., 2017; Burl et al., 2018). We then treated adult rabbits with mirabegron, a β3-AR agonist that also works in rabbits (Figure 4B; Calmasini et al., 2015). Mirabegron-treated rabbits showed a decreasing trend in weight gain (Figure 4C). However, only a few multilocular “brown-like” adipocytes emerged in iBAT after mirabegron treatment (Figure 4D). Gene expression analysis revealed a significant increase in *PPARGC1A* and *PRDM16* mRNA levels, but induction of iBAT *UCP1* by mirabegron was highly variable (Figure 4E), indicating that iBAT in adult rabbits is refractory to adipose beiging stimulated by β3-AR activation.

We then profiled the single-cell expression of iBAT SVF cells from mirabegron-treated rabbits and performed integrated analyses with the 12-week SVF data to identify common cell types (Figure 4F; Table S8; Stuart et al., 2019). Pseudotemporal ordering of the stromal cells predicted two developmental trajectories of *FSTL1*^{intermediate} progenitors (Figure 4G): the default differentiation from group 0 toward group 3 and then group 1 preadipocytes, a fate observed under steady and β3-AR stimulation conditions, and the

alternative but less terminal differentiation toward group 4 and 2 preadipocytes that was specifically induced by mirabegron. Mirabegron-stimulated preadipocytes were able to upregulate feature genes like *FABP4, LPL, APOD, VCAM1*, and *NPR1*, although to a lesser extent compared with classical preadipocytes (Figures 4H and S5C; Table S9). Surprisingly, cells undergoing the alternative path failed to shut down expression of progenitor markers such as *WNT2, DLK1, PI16, DPP4*, and *ANXA3* (Figures 4I and S5C), suggesting that they are not poised for adipogenic maturation. When comparing each stromal population before and after mirabegron treatment, β3-AR activation did not increase the expression of markers for *FSTL1*^{high} brown progenitors (Figure 4J) or decrease the levels of genes that emerged in *FSTL1*^{intermediate} "white" progenitors (Figure 4K). These results show that the *FSTL1*^{intermediate} progenitors in involuted rabbit iBAT adopt a pro-white, anti-brown/beige cell fate.

FSTL1 is a cytokine enriched in brown adipocyte progenitors

Next we set out to explore whether the *FSTL1* gene was functionally important for brown adipocyte progenitors. The encoded glycoprotein follistatin-like 1 belongs to the secreted protein acid and rich in cysteine family, which has a role in lung development, muscle function, and cardioprotection (Mattiotti et al., 2018). However, whether it controls brown adipocyte development and iBAT involution has not been explored. At the RNA level, *FSTL1* was one of the highest expressed gene in total iBAT and sBAT from rabbits (Figure S6A). It colocalized with *bona fide* mesenchymal markers, including *DLK1* and *THY1* at the single-cell level, particularly within neonatal group 2 cells (Figures 5A and 5B), suggesting that *FSTL1*^{high} cells are not likely to be a group of adipogenesis-regulatory cells (Schwalie et al., 2018). At the protein level, FSTL1 showed correlated reduction with UCP1 to minimally detectable levels in total iBAT extracts from 6- and 12-week-old rabbits (Figure 5C).

In humans, the *FSLT1* gene is expressed not just by adipocyte progenitors of fetal iBAT (Figure 3E) but also by preadipocytes from adult deep-neck BAT (Figure S6B), based on a recently published single-nucleus RNA-seq study (Sun et al., 2020). Mature brown adipocytes and non-adipose lineage cells from adult deep-neck BAT had little or no *FSTL1* gene expression (Figure S6B). Notably, SVF cells derived from fetal iBAT and adult deep-neck BAT expressed more FSTL1 protein than those from adult neck WAT (Xue et al., 2015; Wang et al., 2018; Figure 5D).

In preweaning mice, when iBAT is actively growing, FSTL1 expression was the most abundant in total iBAT and the SVF fraction (Figures 5E and 5F). Even though there was a notable reduction in adult mice, FSTL1 protein levels remained high. Compared with inguinal WAT (iWAT), gonadal WAT (gWAT), and skeletal muscle, mouse iBAT possessed the highest level and mostly glycosylated form of FSTL1 (Figure 5G). Fasting, a condition when thermogenic activity is suppressed (Ruan et al., 2014), reduced FSTL1 levels in tissue and serum in mice (Figures 5G-5I). These data imply that the levels of FSTL1 are positively associated with the brown adipogenic ability of SVF cells and the activity of BAT.

During adipogenesis of iBAT SVF cells in culture, FSTL1 protein expression and its secretion were initially upregulated and then diminished when mature brown adipocytes

were induced (Figure 5J). To determine whether *Fstl1*-expressing cells are *bona fide* brown adipocyte progenitors, we generated *Fstl1*^{CreERT2};*Rosa26*$^{mT/mG}$ mice (Figure 5K). A 1-week tamoxifen (TAM) pulse was able to label a fraction of SVF cells as GFP^{+}, as revealed by flow cytometry (Figure 5L) and immunofluorescence (Figure 5M, arrows). No mature brown adipocytes at this stage were labeled. At the 6-week chase, these *Fstl1*$^{+}$ cells differentiated into mature UCP1^{+} brown adipocytes (Figure 5M, asterisks, and Figure S6C). The low labeling was likely due to weak CreERT2 expression downstream of the *Fstl1* gene and a P2A peptide (Liu et al., 2018). Nonetheless, these findings implicate that *Fstl1*$^{+}$ cells are progenitors that can give rise to brown adipocytes.

In support of the notion that FSTL1 is an adipocyte progenitor-enriched cytokine, deleting the *Fstl1* gene in brown/beige adipocytes or all mature adipocytes using *Ucp1*^{Cre} and *Adipoq*^{Cre}, respectively, did not affect levels of FSTL1 protein in iBAT, WAT, or serum (Figures 5N-5S). We did not observe any changes in UCP1 expression (Figures 5O and 5R), body weight, glucose metabolism, or cold-induced thermogenesis in *Ucp1*^{Cre};*Fstl1*$^{fl/fl}$ or *Adipoq*^{Cre};*Fstl1*$^{fl/fl}$ knockout mice (Figures S6D-S6H). On the other hand, using *Myf5*^{Cre} to delete the *Fstl1* gene in embryonic iBAT progenitors (Figure 5T; Timmons et al., 2007), we could achieve ablation of FSTL1 in neonatal iBAT (Figure 5U) and a substantial reduction of serum FSTL1 levels (Figure 5V). These data demonstrate that mature adipocyte-derived FSTL1, if any, is dispensable for BAT development and function.

Loss of *Fstl1* or *Fstl1*-expressing progenitors causes iBAT paucity in young mice

No obvious morphological changes of iBAT during embryonic development were observed in *Myf5-Fstl1* knockout (KO) mice (Figures S7A and S7B). However, neonatal *Myf5-Fstl1* KO mice had less iBAT compared with wild-type littermates (Figure 6A). Expression of the mitochondrial UCP1 and COX4 proteins was attenuated (Figure 5U). There was barely any lipid deposition in *Myf5-Fstl1* KO iBAT (Figure 6B). As a result, *Myf5-Fstl1* KO pups could not maintain their body temperature when separated from dams (Figure 6C) and died within a few days after birth, probably because of hypothermia and muscle dysfunction (suggested by a hunched posture).

Housing mice at thermoneutrality extended the survival of *Myf5-Fstl1* KO pups (Figure 6D) and restored lipid content in iBAT (Figure 6E). An assessment of the iBAT morphology at thermoneutrality showed that *Myf5-Fstl1* KO iBAT did not increase its mass from days 1–7 (Figure 6F). The reduction in mass was specific to iBAT (Figure 6G) because other critical organs, including the liver, heart, and hindlimbs, and head-to-body weight ratio was not affected (Figure S7C). We then used novel markers identified from scRNA-seq of rabbit SVF cells (Figure 2) for flow cytometry assays. In *Myf5-Fstl1* KO iBAT from newborns, the frequencies of lineage-negative SFRP4^{+} brown adipocyte progenitors and VCAM1^{+} and PDGFRA^{+}NRP1^{+} committed preadipocytes were comparable with wild-type littermates (Figure S7D). However, at post-natal day 7 (survival of KO mice was extended by reducing the litter size), adipocyte progenitors and preadipocytes had significantly reduced numbers in *Myf5-Fstl1* KO pups (Figure 6H). To investigate whether FSTL1 acts in a cell-autonomous manner, we cultured *Fstl1*$^{fl/fl}$ iBAT SVF cells and knocked down the *Fstl1* gene using a Cre-expressing lentivirus. FSTL1 knockdown did not affect adipogenic

differentiation; however, thermogenic genes, including *Ucp1, Dio2, Ppargc1a*, and *Prdm16*, were specifically downregulated (Figure 6I). These results demonstrate that FSTL1 deletion in adipose progenitors causes brown adipogenic incompetence and iBAT paucity in mice.

Muscle defects persisted in *Myf5-Fstl1* KO mice at the thermoneutral zone (data not shown), presumably eventually causing mortality. However, the iBAT defects observed in *Myf5-Fstl1* KO mice were not results of the loss of skeletal muscle-derived FSTL1 because deleting FSTL1 in skeletal myocytes using the HSA^{Cre} line did not affect postnatal survival (Miyabe et al., 2014), iBAT morphology, UCP1 expression (Figures 6J-6L), body weight, or glucose metabolism (Figures S7E and S7F).To determine whether $Fstl1^{+}$ brown adipocyte progenitors are required for the BAT identity in adult mice, we generated $Fstl1^{CreERT2}$;$Rosa26^{DTR}$ mice, induced Cre expression by TAM, and acutely ablated *Fstl1*-expressing cells by diphtheria toxin (DT) (Figure 6M). 5 weeks after DT ablation, UCP1 protein levels were reduced in iBAT (Figure 6N). As a result, $Fstl1^{CreERT2}$;$Rosa26^{DTR}$ mice were more sensitive to cold-induced body temperature reduction compared with control animals (Figure 6O). Less weight loss after cold challenge was observed (Figure 6P), also indicative of reduced energy expenditure. Therefore, $Fstl1^{+}$ progenitors are functionally important for BAT thermogenesis.

FSTL1 sustains WNT signaling in brown adipocyte progenitors

iBAT paucity in *Myf5-Fstl1* KO mice was not due to defects in sympathetic nerve innervation, tissue vascularization, or macrophage polarization (Figures S8A-S8C). We also bred the mice to a Cre-dependent reporter line and found that adipocytes in *Myf5-Fstl1* KO iBAT were still derived from the *Myf5* lineage (Figure S8D), suggesting no evocation of progenitor cell plasticity nor recruitment of alternative origins of brown adipocytes. RNA-seq of total iBAT found 505 upregulated and 308 downregulated genes in *Myf5-Fstl1* KO mice (Table S10). Adipogenic and thermogenic pathways were enriched in downregulated genes, whereas inflammatory and immune-activating genes were upregulated (Figures 7A and 7B). Gene set enrichment analysis (GSEA) identified that β-catenin-controlled genes were overrepresented in the downregulated gene set (Figure 7C). WNT/β-catenin signaling promotes self-renewal of stem cells, including adipocyte progenitors, but inhibits adipogenic differentiation (Kang et al., 2005; Lo et al., 2016). The mesenchymal marker *DLK1* is a WNT target gene (Paul et al., 2015). *GPC3*, another brown adipocyte progenitor marker identified in this study, facilitates and/or stabilizes the interaction of WNTs with Frizzled receptors (Niehrs, 2012; Capurro et al., 2014). We wanted to determine whether FSTL1 sustains activation of WNT signaling in brown adipocyte progenitors.

By interrogating BioPlex 2.0, a database of protein-protein interactions (Huttlin et al., 2017), we found that FSTL1 binds to several WNT proteins (Table S11). Co-immunoprecipitation validated that FSTL1, regardless of glycosylation status, physically interacted with WNT10B (Figure 7D) as well as GPC3 (Figure 7E). In group 2 rabbit brown adipocyte progenitors, the *FSTL1* gene was mostly co-expressed with *WNT2* and *GPC3* (Figures 7F and 7G). Similar to *DLK1, FSTL1* expression was dependent on β-catenin because XAV939, an inhibitor of tankyrase 1/2 that suppresses β-catenin activity, reduced FSTL1 protein levels in SVF cells (Figure 7G). As a result, WNT10B-stimulated SVF proliferation

was ablated when FSTL1 was absent (Figures 7I and S8E). Constitutive expression of WNT10B suppressed brown adipogenic differentiation (Kang et al., 2005). FSTL1 knockdown specifically attenuated suppression of thermogenic genes (*Ucp1* and *Prdm16*), but not general adipogenic genes (*Adipoq, Fabp4*, and *Pparg*), by WNT10B (Figure 7J). On the other hand, β-catenin inhibition by XAV939 increased UCP1 protein expression, which was diminished by FSTL1 overexpression (Figure 7K). These data implicate that the synchronized action of FSTL1 and WNT sustains the iBAT progenitor cell pool and brown adipogenic competence (Figure 7L). However, doxycycline-induced FSTL1 overexpression in 12-week rabbit SVF cells failed to reactivate UCP1 protein expression in culture (Figure S8F), suggesting that FSTL1 is required but not sufficient to re-establish the browning capacity of involuted BAT progenitor cells.

DISCUSSION

The fact that human BAT, including periscapular, perijugular, and perirenal depots, undergoes age-related involution/atrophy raises doubts about the physiological significance of this organ in humans. Activating residual (if any are left) brown and/or beige adipocytes in midlife to late life might have limited metabolic benefits; however, preventing/delaying BAT involution or regenerating BAT via cell-based therapies may offer the potential to combat metabolic diseases. Our study here is one of the first attempts to understand the nature and mechanisms of BAT involution.

BAT involution is not unique to humans and has been observed in large mammals such as sheep, bovines, and rabbits (Derry et al., 1972; Gemmell et al., 1972; Casteilla et al., 1989; Basse et al., 2015; Oelkrug et al., 2015). Studies with rodents have proposed several mechanisms for age-associated functional decline of brown and beige fat. Impairment of sympathetic input, altered endocrine control, and tissue inflammation during aging contribute to thermogenic dysfunction (Graja et al., 2019; Zoico et al., 2019). Adipocyte-intrinsic mechanisms include reduced UCP1 expression and activity (Horan et al., 1988; McDonald et al., 1988; Florez-Duquet et al., 1998), cellular senescence (Berry et al., 2017), and mitochondrial lipoylation (Tajima et al., 2019). However, it is unclear whether these deteriorations, which normally happen in late life, also play a part in BAT involution during early life, particularly in larger animals, including humans and rabbits.

Recent data suggest that brown adipocyte thermogenesis in humans is driven by β2-AR stimulation (Blondin et al., 2020). In rabbits, all βAR genes (*ADRB1, ADRB2*, and *ADRB3*) are expressed in iBAT, with *ADRB3* showing the highest expression and the most reduction during involution. In the SVF compartment, *ADRB2* expression is about 10-fold more than that of *ADRB1* and *ADRB3*, indicating that rabbit β2-AR signaling might support progenitor function and brown adipogenesis, whereas β3-AR signaling is more involved in mature adipocyte fate maintenance and BAT involution. Such selective utilization of βAR signaling upon diverse environmental stimuli has also been observed in mice (Jiang et al., 2017). Our observations of age-dependent downregulation of βAR genes and upregulation of αAR genes indicate that inactivation of Gs-coupled, pro-thermogenic signaling and activation of Gi-coupled, thermogenesis-in-hibiting signaling would support BAT involution. Altered AR expression patterns, combined with an increase in sympathetic

innervation, suggest that BAT involution in rabbits has intrinsic causes. This conclusion is further supported by the following observations. (1) Rabbit SVF cells from involuted iBAT maintain the impairment in brown adipogenesis when transplanted into the dorsal region of young mice, an environment without age-related BAT dysfunction. (2) Cold and βAR agonist treatments do not recruit $UCP1^{+}$ brown adipocytes.

The contribution of adipocyte progenitors to BAT whitening has been suggested by studies in mice. The turnover rate of brown adipocytes at room temperature and thermoneutrality is low but evident (Moser et al., 2021). Although contributing minimally to BAT recruitment during cold (Lee et al., 2015), brown adipose progenitors are essential for adipocyte regeneration after tissue damage (Sakaguchi et al., 2017; Moser et al., 2021). Deleting transcriptional regulators such as PRDM16, EBF2, and BCL2 only in *Myf5* progenitors but not mature adipocytes leads to white fat-like morphology and severe thermogenic defects in adulthood (Harms et al., 2014; Shapira et al., 2017; Kutyavin and Chawla, 2019), emphasizing the essentiality of progenitor competence in maintaining BAT identify. Here, using $Fstl1^{CreERT2}$-mediated cell ablation, we also showed that loss of brown adipocyte progenitors can contribute to BAT dysfunction in young mice. Future experiments are required to determine the quantitative role of adipocyte progenitors in age-dependent BAT involution and dysfunction.

In contrast to humans and rabbits, mice have constitutively high levels of FSTL1 expressed by brown adipocyte progenitors. This can be a potential mechanism to support the life-long existence and activity of BAT in mice to cope with the high thermogenic demand. Recently, using whole-body heterozygous $Fstl1^{+/-}$ mice, we showed that FSTL1 is required for optimal BAT recruitment during cold and after β3-adrenergic activation (Fang et al., 2019). The thermogenic effect of FSTL1 cannot be attributed to mature brown adipocytes because its expression and secretion were downregulated during adipogenic differentiation, and no changes in FSTL1 expression or BAT function were observed in $Ucp1^{Cre};Fstl1^{fl/fl}$ and $Adipoq^{Cre};Fstl1^{fl/fl}$ KO mice. Only deletion of FSTL1 in $Myf5^{+}$ cells diminished brown adipose progenitors and caused iBAT paucity and thermogenic defects in mice. FSTL1 is also expressed in WAT, at a level much lower than BAT. It is transiently induced during adipogenic differentiation of 3T3-L1 cells and then rapidly downregulated to background levels (Wu et al., 2010; Fang et al., 2019). Intriguingly, knocking down *Fstl1* or treatment with high levels of recombinant FSTL1 interferes with 3T3-L1 differentiation (Prieto-Echague et al., 2017). scRNA-seq data suggest FSTL1 as an enriched factor for mesenchymal cells in various tissues (Tabula Muris et al., 2018). We speculate that FSTL1 can potentially function to sustain the renewal and competence of diverse mesenchymal stem/progenitor cells.

FSTL1 is involved in multiple signaling pathways; in particular, it inhibits bone morphogenetic protein (BMP) signaling by competitively binding to BMP4 (Geng et al., 2011). BMP signaling promotes commitment of mesenchymal stem cells into the adipogenic lineage (Tang and Lane, 2012). It would be counterintuitive for FSTL1 in BAT to inhibit BMP signaling, which would predict increased adipogenic commitment and differentiation in $Myf5^{Cre};Fstl1^{fl/fl}$ KO mice. Instead, bioinformatics analysis of differentially expressed genes pointed to reduced WNT/β-catenin activity, which has been shown extensively to

promote the proliferation and competence of progenitor cells (Prestwich and Macdougald, 2007). FSTL1 physically interacts with WNT10B *in vitro* and acts downstream of WNT10B to balance the proliferation and differentiation of SVF cells. Another common maker of human and rabbit *FSTL1*^{high} progenitors we identified in this study is *GPC3*, which encodes a heparan sulfate proteoglycan that binds to the outer surface of the plasma membrane (Filmus et al., 2008) and facilitates interaction of WNTs with Frizzled receptors (Niehrs, 2012; Capurro et al., 2014). It is tempting to speculate that brown adipocyte progenitors in mice self-sustain WNT signaling to support their functional competence by establishing a FSTL1/GPC3-dependent feedforward circuit (Figure 7M).

We propose that rabbits mimic the age-dependent process of BAT involution observed in humans much more closely than mice. Brown adipocyte progenitors in iBAT of humans, rabbits, and mice highly express FSTL1. Age-dependent transcriptional remodeling and identity switching of interscapular fat in rabbits is associated with functional incompetence of adipocyte progenitors and downregulation of FSTL1. Loss of FSTL1 in brown adipocyte progenitors attenuates WNT signaling and drives iBAT paucity in mice. Our data could potentially inform future development of preventive and regenerative medicine in obesity and comorbidities.

Limitations of the study

BAT involution is undoubtedly a multifactorial process involving parenchymal adipocytes, sympathetic nerves, and resident immune and other supporting cells. The current study primarily investigated the contribution of adipocyte progenitor cells. How the progressive restriction in progenitor competence cooperates with other mechanisms in BAT involution is unknown. The ultimate fate of preexisting *FSTL1*^{high} adipocyte progenitors is also still unknown: do they become extinct or transdifferentiate into *FSTL1*^{intermediate} progenitors? It is of high importance to develop genetic rabbit models and perform fate-mapping experiments to uncover these possibilities. BAT is exceptionally heterogeneous in development, metabolism, and function (Ruan, 2020), and it will not be surprising to find that there are depot-specific determinants of BAT involution. We will determine whether progenitor restriction and loss of *FSTL1* are associated with the involution process of other BAT depots. Although FSTL1 is essential for BAT development, and its loss leads to BAT paucity in mice, restoration of FSTL1 expression in involuted BAT progenitors is not sufficient to drive their differentiation toward UCP1^{+} brown adipocytes. Future efforts are demanded to identify potential master regulators that are capable of reprogramming progenitor fate and rejuvenating aged BAT for translational medicine.

STAR★METHODS

RESOURCE AVAILABILITY

Lead contact—Requests for further information and resources can be directed to the lead contact, Hai-Bin Ruan (hruan@umn.edu).

Materials availability—Plasmids generated in this study are available upon request.

Data and code availability—RNA-seq data reported in this paper have been deposited in the Gene Expression Omnibus with the accession numbers GEO: GSE148888 and GEO: GSE148891. Original western blot images and microscopy data reported in this paper will be shared by the lead contact upon request.

This paper does not report original code.

Any additional information required to reanalyze the data reported in this paper is available from the lead contact upon request.

EXPERIMENTAL MODEL AND SUBJECT DETAILS

Animals—All animal experiments were approved by the institutional animal care and use committee of the University of Minnesota. All the mice group-housed in light/dark cycle- (6am-8 pm light), temperature- (21.5 ± 1.5°C), and humidity-controlled (30-70%) room, and free to access water and regular chow (Teklad #2018) unless otherwise indicated. All mice were maintained on a C57BL6 background. *Fstl1*$^{fl/fl}$ mice (#B000172) were a kind gift from Dr. Xu Zhang. *Fstl1-CreER* were a kind gift from Dr. Wen Ning. *UCP1-Cre* (#024670), *Myf5-Cre* (#007893), *HAS-Cre* (#006149), *Adipoq-Cre* (#010803), *Rosa26-mTmG*(#007676), and *Rosa26-DTR*(#007900) were purchased from the Jackson laboratory. For *UCP1*^{Cre}*:Fstl1, Adipoq*^{Cre}*:Fstl1, HSA*^{Cre}*:Fstl1* animals, female *Fstl1*$^{fl/fl}$ mice were bred with male *Fstl1*$^{fl/fl}$*:Cre* mice to get age- and sex-matched pairs for experiments. For *Myf5*^{Cre}*:Fstl1* animals, *Fstl1*$^{fl/fl}$ females were inbreeded with *Fstl1*$^{fl/+}$*:Myf5-Cre* males. *CreERT2* expression was induced by feeding mice with tamoxifen food (Envigo TD.130860) for 1 week. Both male and female mice were used in the study. If not specified, mixed-sex animals were used.

Male and female 6-week and 12-week old New Zealand White rabbits were purchased from Bakkom Rabbitry and individually housed in a temperature- (19 ± 1°C) and humidity-controlled (30-70%) room with *ad libitum* access to food (Envigo, #2031) and water. To obtain newborn and 3-week-old rabbit kids (mixed sexes), pregnant does were purchased and individually housed as indicated above, fed with a different food (Envigo, #2030).

Human subjects—Human interscapular BAT tissue was obtained at Nanjing Maternity and Child Health Care Hospital (Nanjing, China) from an induction aborted fetus with congenital heart disease at the gestational age of 24 weeks. Written informed consent was signed by parents. This study was approved by the Medical Ethics Committee of Nanjing Maternity and Child Health Care Hospital (Permit number: [2019] KY-081) and complied with the Population and Family Planning Law of China.

METHOD DETAILS

Human cell culture—Human hTERT A41hBAT-SVF and hTERT A41hWAT-SVF cells were maintained in DMEM containing 10% FBS and 1% Pen-Strep. Primary human fetal iBAT SVF cells were maintained in Adipocyte Medium and experiments were on cells with less than 5 passages. HEK 293FT cells were maintained in DMEM containing 10% FBS and 1% Pen-Strep.

Mouse SVF isolation, culture, immortalization, and differentiation—iBAT depots from six 1-month-old mice were collected, pooled and minced in 10 mL of digestion buffer (DMEM/F12 with 1 mg/mL Collagenase I, 1% FBS, 1% HEPES, and 1% Pen-Strep). After shaking in 37°C at 100 rpm for 45 min, digested tissues were filtered thought 70-μm strainers and centrifuged at 1500 rpm for 3 min. The pellets were resuspended in ACK buffer and put on ice for 5 min to remove red blood cells. The ACK buffer was neutralized with 5 mL of DMEM/F12 plus 10% FBS and removed after a 1500 rpm centrifugation for 3 min. SVF cells were seeded in a 60-mm dish with DMEM/F12 containing 20% FBS, 1% Pen-Strep, and 10 μg/mL Ciprofloxacin. After 12 h, adherent SVF cells were infected with lentivirus expressing CMV-SV40T-P2a-Blasticidin. When confluent, infected SVF cells were passed into a 10-cm dish, cultured with DMEM/F12 (10% FBS, 1% Pen-Strep, 10 μg/mL Blasticidin), and labeled as passage 1 (P1). After an additional subculture, the immortalized P2 SVF cells were harvested into 10 cryogenic vials from a 15-cm dish for cryopreservation in liquid nitrogen. Cells with less than 5 passages were used.

For adipogenic differentiation, confluent cells were induced with DMEM/F12 containing 10% FBS, 1x Pen-Strep, 20 nM insulin, 1 nM T3, 0.5 mM IBMX, 5 μM dexamethasone, and 125 μM indomethacin. Two days later, cells were maintained in DMEM/F12 containing 10 %FBS, 1x Pen-Strep, 20 nM insulin, and 1 nM T3. Medium was changed every other day until lipid droplets appeared.

Rabbit SVF isolation, culture, and differentiation—Rabbit BAT SVF cells were isolated following the aforementioned mouse protocol, without immortalization and Pen-Strep was changed to Primocin. For “brown” adipogenic differentiation, cells were cultured in DMEM/F12 with 10% FBS and 1X Primocin until confluent, induced with DMEM/F12 containing 2% FBS, 1X Primocin, 3.5 μg/mL insulin, 1 nM T3, 0.5 mM IBMX, 5 μm dexamethasone, 125 μm indomethacin, 33 μm biotin, 10 μg/mL transferrin, 17 μm pantothenate, 1 μm rosiglitazone, 50 μm 2-DG. The medium was changed once 2 days later. Afterward, cells were maintained in DMEM/F12 with 2% FBS, 1X Primocin, 3.5 μg/mL insulin, 1 nM T3, 1 μm rosiglitazone, changed every other day until lipid droplets appeared.

For “white” adipogenic differentiation, SVF cells were induced with DMEM/F12 containing 2% FBS, 1X Primocin, 3.5 μg/mL insulin, 0.5 mM IBMX, 5 μM dexamethasone, 33 μM biotin, 10 μg/mL transferrin, 17 μM pantothenate, 50 μM 2-DG for 4 days, and then changed into DMEM/F12 with 2% FBS, 1X Primocin, 3.5 μg/mL insulin for another 4 days. All medium was changed every 48 h.

Seahorse respirometry—Oxygen consumption rate (OCR) was measured using the Seahorse XFe96 Analyzer (Agilent) on day 8 of differentiation. One hour prior to respirometry, media was replaced with basal DMEM (Sigma Aldrich D5030) supplemented with 5 mM glucose, 2 mM GlutaMax TM (Fisher Scientific 13462629) and 2% fatty acid-free BSA (Sigma Aldrich A3803), and cells were incubated at 37°C in a non-CO2 incubator. NE (final concentration 2 μM) was injected to stimulate brown adipocytes. ATP-linked respiration and uncoupling were determined by injecting Oligomycin (final concentration 5 μM) and Antimycin A (final concentration 5 μM) respectively. Basal mitochondrial respiration in stimulated cells was determined by subtracting the non-mitochondrial

respiration from NE-induced OCR. Raw data were normalized by *in situ* nuclear staining (Hoechst 33342, final concentration 10 μM) and *in situ* cell counting using Seahorse XF Imaging and Normalization system (Agilent). Normalized data were used for calculations.

Matrigel implantation—Rabbit SVF cells were cultured in DMEM/F12 with 10% FBS and 1X Primocin until being confluent. Cells were then washed with PBS and detached with trypsin-EDTA at 37°C for 5 min. After neutralized with culture medium, 10^7 cells were pelleted at 300 g for 3 min, resuspended in 1 mL of Matrigel, kept on ice, and injected subcutaneously into the back of a 6-week-old NCG mouse with an insulin syringe. Slowly retrieve the needle during injection to obtain a flat implantation.

β3 adrenergic receptor agonism—Mirabegron stock was prepared in DMSO at 175 mg/mL. 900 μL mirabegron stock was further dissolved in 44.1 mL of 5% Kolliphor EL solution and filtered through a 0.22-μm filter. Rabbits received daily intraperitoneal injections at 3.5 mg/kg body weight for 14 days.

Glucose and insulin tolerant tests—For glucose tolerance test, 16 h-fasted mice were intraperitoneally injected with glucose (20% in saline, 1.5 g/kg body weight). Blood glucose from tail-vein blood collected at the designated times was measured using a Bayer Contour Glucometer. For insulin tolerant test, mice were fasted for 6 h, and blood glucose was recorded after Insulin (100 IU/μL, 0.75 IU/kg body weight) was injected intraperitoneally.

Body temperature—To measure skin temperature of mice, pups were separated from dams, briefly placed in a 30°C incubator, followed by the mild cold challenge at 22°C for 3 h. Pictures were taken with a FLIR-C2 thermal camera and peri-scapular skin temperature was measured with the FLIR tool. To measure rectal temperature during cold challenge, individually housed mice were placed in their home cages at 4°C, with free access to food and water. A fully lubricated rectal probe (Physitemp) was used to record core body temperature at indicated time points.

Histology—Adipose tissues were fixed in formalin solution at 4°C for 24 h. Tissue embedding, sectioning, and hematoxylin and eosin staining were performed at the Comparative Pathology Shared Resource of the University of Minnesota. For immunostaining, antigen retrieval was performed in Citric buffer using a 2100 Retriever (Aptum Biologics). After incubation with blocking buffer (3% BSA in PBS) for 1 h, sections were immersed with primary antibody in blocking buffer overnight at 4°C. For immunohistochemistry, slides were rinsed with PSB for 3 times, then labeled with Histostain®-Plus 3rd Gen IHC Detection Kit next day. For immunofluorescence, PBS-washed slides were incubated with an fluorescent secondary antibody at room temperature for 1 h, and then mounted with VECTASHIELD® Antifade Mounting Medium with DAPI after three times of PBS wash. A Nikon system was used for imaging.

Real-time RT-PCR—RNA was isolated with Trizol and reverse transcribed into cDNA with the iScript™ cDNA Synthesis Kit. Real-time RT-PCR was performed using iTaq™ Universal SYBR® Green Supermix and gene-specific primers on a Bio-Rad C1000 Thermal Cycler.

MTT assay—1000 cells were initially seeded into one well on a 96-well plate with 100 μL DMEM/F12 plus 2% FBS and MTT assays were performed at indicated time points. Briefly, 10 μL of MTT (5 μg/μL) was added into each well. After incubation at 37°C for 3 h, liquid was removed, and 100 μL DMSO was added to dissolve the MTT formazan. The absorbance was read at 590 nm.

Lentivirus packaging—HEK 293FT cells were seeded into 60-mm dishes a night before the experiment to get 70% confluence at transfection. For a 60-mm dish, the culture medium was replaced with 4 mL of fresh DMEM containing 2% FBS 1 h before transfection. 2 μg transfer plasmid, 1.5 μg pSPAX2, 0.5 μg pMD2G were mixed with 16 μL PEI Max solution (1 mg/mL) in 0.5 mL of 0.9% NaCl and set in room temperature for 20 min to form the transfection complex. After being incubated with cells for 6 h, the transfection complex was replaced with 5 mL DMEM plus 10% FBS. The medium containing lentivirus was collected every 24 h for 3 days, filtered thought a 0.45-μm PVDF filter, and kept at −80°C until use.

Co-immunoprecipitation—293FT cells cultured in 6-mm dishes were transfected with 2 μg pLXSN2-WNT10b-HA and 2 μg pLVX-FSTL1-Myc (WT or MT). 48 h later, protein was extracted with 1400 μL NP-40 lysis buffer. 2 μg antibody (Myc, HA, or Normal rabbit IgG) and 15 μL Protein A/G beads were added into 400 μL protein lysate and incubated overnight at 4°C. Protein A/G beads were washed with TBS for 3 times, boiled with 2x Laemmli buffer, and subjected to Western blotting.

Flow cytometry—SVF cells from mouse iBAT were isolated as described above. Each iBAT depot was lysed with 3 mL Collagenase I buffer in individual tubes and fileted with a 40-μm filter. SVF cells were stained with primary antibody at 1:100 dilution on ice for 30 min. For SFRP4, SVF cells were then stained with an anti-rabbit IgG-AF647 secondary antibody (1:200 dilution) for another 30 min. Fixable Viability Dye was used to exclude dead cells as instructed by the manufacturer. Flow cytometry was performed on an LSR Fortessa H0081 or X20 and analyzed with FlowJo.

Bulk RNA-seq and longitudinal analyses—RNA of total BAT depots or SVF cells from rabbits or mice was isolated with PureLink™ RNA Mini Kit, following the manufacturer's instruction. RNA quality was determined by an Agilent 2100 Bioanalyzer. Library was prepared at BGI and sequencing was performed using the BGISEQ-500 platform. Reads were filtered with SOAPnuke and mapped to genome with HISAT2. Clean reads were mapped to the mm10 reference with Bowtie2 and gene expression levels were determined with RSEM. Differentially expressed genes were detected using DEseq2 with the following parameters: fold change >= 2.00 and adjusted p-value <= 0.05. The longitudinal analysis was implemented using the log10-transformed FPKM (Fragments Per Kilobase Million) and considering Tukey's method with null hypotheses for each longitudinal pattern. For example, if simultaneous hypothesis testing of two null hypotheses "D1 – W3 ≥ 0" and "W3 – W6 ≥ 0" are rejected, they are determined as the genes with "continued up-regulation" (D1 < W3 < W6). Candidate gene prioritization and pathway analysis were performed using the online ToppGene Suite.

Rabbit SVF scRNA-seq and analyses—Rabbit iBAT depots were dissected at indicated ages and minced with sharp scissors in Liver Digest Medium (Thermo Fisher, 2 mL/g tissue). After shaking in 37°C at 100 rpm for 30 min, the digestion mix was centrifuged at 300 rpm for 10 min at 4°C. The pellet was resuspended in 5 mL ACK buffer and placed on ice for 5 min. After being neutralized with 5 mL of DMEM/F12 plus 10% FBS, SVF cells were filtered thought a 40-μm strainer, and pelleted by centrifugation at 300 rpm for 10 min at 4°C. SVF cells were then treated with a Dead cell removal kit (Miltenyi Biotec) and immediately subjected to single-cell library preparing with the 10X Genomics platform and a Chromium Single Cell 5′ Reagent Kit at the University of Minnesota Genomics Center. Sequencing of the library (paired-end 100 bp) was performed on an Illumina NovaSeq 6000 instrument. The raw data were processed using the 10x Genomics Cell Ranger package (version 3.0.1). The rabbit transcriptome was generated by filtering genome assembly (Oryctolagus_cuniculus.OryCun2.0.dna.toplevel.fa) for protein-coding genes defined in GTF file (Oryctolagus_cuniculus.OryCun2.0.94.gtf).

Seurat (v3.1.5) on RStudio were used to merge SVF cells from rabbits of different age, to filter cells with >1000 detected genes and < 5% of genes mapped to mitochondria; to normalize data with the SCTransform function to regress out variables including mitochondrial mapping percentage, ribosomal mapping percentage and sample batches; and to cluster cells (dims = 1:30, resolution = 0.2). UMAP and tSNE were then used for two-dimensional visualization of the resulting cluster. Marker genes were identified using the FindAllMarkers function (only.pos = TRUE, min.pct = 0.25, logfc.threshold = 0.25). Violin plots, dot plots, heatmaps, and individual tSNE and UMAP plots for the given genes were generated by using the VlnPlot, DotPlot, DoHeatmap, and FeaturePlot functions, respectively. To visualize co-expression of two features simultaneously, FeaturePlot with blend was used (blend = TRUE, blend.-threshold = 0, order = TRUE, min.cutoff = "q10″, max.cutoff = "q90″). Integration analyses with Seurat were performed for 12-week and Mirabegron-treated SVF cells. For pseudotime analysis, stromal cell clusters were filtered and converted to a CellDataSet in Monocle 3. A trajectory was built and pseudotime was computed by set *DLK1*^{high} *WNT2*^{high} progenitors as the root.

Human SVF scRNA-seq and analyses—Human fetal iBAT was digested with Collagenase I buffer (2 mL/g tissue). Collagenase I buffer was freshly prepared (44.5 mL DMEM/F12, 2 mL of 20 mg/mL collagenase I in HBSS, 500 μL HEPES, 500 μL FBS, 500 μL Pen-Strep, and sterilized with a 0.22-μm filter). After minced into 1 mm^3 pieces, tissue was shaken at 37°C at 150 rpm for 45 min and then centrifuged at 1500 rpm for 3 min. The pellet was suspended in 5 mL ACK buffer and incubated on ice for 5 min to remove red blood cells. 10 mL of DMEM/F12 with 10% FBS was added to neutralize the ACK buffer. Cells were then filtered thought a 40-μm strainer, followed by centrifugation at 1500 rpm for 3 min. The pellet was resuspended in FBS with 10% DMSO, aliquoted into 1 mL per tube, frozen in a Mr. Frosty Freezing Container (Thermo Fisher Scientific) at −80°C. and then shipped to BGI on dry ice. Upon receiving, the SVF cells were rapidly resuscitated in 37°C water bath. After sorting with Dead cell removal kit (Miltenyi Biotec), live SVF cells were used for library construction using the Chromium Controller and Chromium Single Cell 3′ Reagent Kit (10X Genomics). The library was sequenced using an BGISEQ-500 instrument.

FASTQ reads were processed and converted to digital gene expression matrices after mapping to the mm10 reference genome using the Cell Ranger Single Cell Software Suite (v3.1.0). Seurat (v3.1.5) was used to trim dataset (nFeature_RNA >200, nFeature_RNA <6380, percent.mt < 5), normalize data (LogNormalize). Highly variable genes were used for principal component analysis, followed by clustering in PCA space using a graph-based clustering approach (dims = 1:10, resolution = 0.5). UMAP and tSNE were then used for two-dimensional visualization of the resulting cluster. Marker genes were identified using the FindAllMarkers function (only.pos = TRUE, min.pct = 0.25, logfc.threshold = 0.25).

QUANTIFICATION AND STATISTICAL ANALYSIS

Results are shown as mean ± SEM. N values and statistical analysis methods are described in figure legends. The statistical comparisons were carried out using two-tailed unpaired Student's t test and one-way or two-way ANOVA with indicated post hoc tests with Prism 7 (Graphpad). Differences were considered significant when $p < 0.05$. *, $p < 0.05$; **, $p < 0.01$; ***, $p < 0.001$.

Supplementary Material

Refer to Web version on PubMed Central for supplementary material.

ACKNOWLEDGMENTS

We thank Dr. Maria Razzoli and Dr. Pilar Ariza Guzman for EchoMRI and CLAMS analyses; Dr. Xiang Gao, Dr. Xu Zhang, and Dr. David Broide for providing the *Fstl1-floxed* mice; Dr. Yu-Hua Tseng for providing immortalized human brown preadipocytes and suggestions; and Dr. Chenbo Ji for providing embryonic human brown preadipocytes. This work was supported by the National Natural Science Foundation of China (32170847), the National Key R&D Program of China (2017YFD0500505), the Natural Science Foundation of Jiangsu Province (BK20150687), and China Scholarship Council postdoctoral fellowship (201606855010) (to Z.H.). This work was also supported by the Natural Science Foundation of Jiangsu Province (BK20170147 to Z.Z.), the NIH/NIDDK (R56 DK118150 to A.B.), and the American Diabetes Association (18-IBS-167) and NIH/NIAID (R01 AI139420 and R21 AI140109 to H.-B.R.). H.N. and S.S. were supported by NIH grants UL1 TR002494 and R01 AI148669.

REFERENCES

Basse AL, Dixen K, Yadav R, Tygesen MP, Qvortrup K, Kristiansen K, Quistorff B, Gupta R, Wang J, and Hansen JB (2015). Global gene expression profiling of brown to white adipose tissue transformation in sheep reveals novel transcriptional components linked to adipose remodeling. BMC Genomics 16, 215. [PubMed: 25887780]

Berry DC, Jiang Y, Arpke RW, Close EL, Uchida A, Reading D, Berglund ED, Kyba M, and Graff JM (2017). Cellular aging contributes to failure of cold-induced beige adipocyte formation in old mice and humans. Cell Metab. 25, 481. [PubMed: 28178569]

Blondin DP, Nielsen S, Kuipers EN, Severinsen MC, Jensen VH, Miard S, Jespersen NZ, Kooijman S, Boon MR, Fortin M, et al. (2020). Human Brown adipocyte thermogenesis is driven by β2-AR stimulation. Cell Metab. 32, 287–300.e7. [PubMed: 32755608]

Burl RB, Ramseyer VD, Rondini EA, Pique-Regi R, Lee YH, and Granneman JG (2018). Deconstructing adipogenesis induced by beta3-adrenergic receptor activation with single-cell expression profiling. Cell Metab. 28, 300–309.e4. [PubMed: 29937373]

Calmasini FB, Candido TZ, Alexandre EC, D'Ancona CA, Silva D, de Oliveira MA, De Nucci G, Antunes E, and Monica FZ (2015). The beta-3 adrenoceptor agonist, mirabegron relaxes isolated prostate from human and rabbit: new therapeutic indication? Prostate 75, 440–447. [PubMed: 25417911]

Cambon B, Reyne Y, and Nougues J (1998). In vitro induction of UCP1 mRNA in preadipocytes from rabbit considered as a model of large mammals brown adipose tissue development: importance of PPARgamma agonists for cells isolated in the postnatal period. Mol. Cell Endocrinol 146, 49–58. [PubMed: 10022762]

Cannon B, and Nedergaard J (2004). Brown adipose tissue: function and physiological significance. Physiol. Rev 84, 277–359. [PubMed: 14715917]

Cao J, Spielmann M, Qiu X, Huang X, Ibrahim DM, Hill AJ, Zhang F, Mundlos S, Christiansen L, Steemers FJ, et al. (2019). The single-cell transcriptional landscape of mammalian organogenesis. Nature 566, 496–502. [PubMed: 30787437]

Capurro M, Martin T, Shi W, and Filmus J (2014). Glypican-3 binds to Frizzled and plays a direct role in the stimulation of canonical Wnt signaling. J. Cell Sci 127, 1565–1575. [PubMed: 24496449]

Casteilla L, Champigny O, Bouillaud F, Robelin J, and Ricquier D (1989). Sequential changes in the expression of mitochondrial protein mRNA during the development of brown adipose tissue in bovine and ovine species. Sudden occurrence of uncoupling protein mRNA during embryogenesis and its disappearance after birth. Biochem. J 257, 665–671. [PubMed: 2930477]

Cui X, Nguyen NL, Zarebidaki E, Cao Q, Li F, Zha L, Bartness T, Shi H, and Xue B (2016). Thermoneutrality decreases thermogenic program and promotes adiposity in high-fat diet-fed mice. Physiol. Rep 4, e12799. [PubMed: 27230905]

de Jong JMA, Sun W, Pires ND, Frontini A, Balaz M, Jespersen NZ, Feizi A, Petrovic K, Fischer AW, Bokhari MH, et al. (2019). Human brown adipose tissue is phenocopied by classical brown adipose tissue in physiologically humanized mice. Nat. Metab 1, 830–843. [PubMed: 32694768]

Derry DM, Morrow E, Sadre N, and Flattery KV (1972). Brown and white fat during the life of the rabbit. Dev. Biol 27, 204–216. [PubMed: 5019935]

Fang D, Shi X, Lu T, Ruan H, and Gao Y (2019). The glycoprotein follistatin-like 1 promotes brown adipose thermogenesis. Metabolism 98, 16–26. [PubMed: 31132382]

Filmus J, Capurro M, and Rast J (2008). Glypicans. Genome Biol. 9, 224. [PubMed: 18505598]

Florez-Duquet M, Horwitz BA, and McDonald RB (1998). Cellular proliferation and UCP content in brown adipose tissue of cold-exposed aging Fischer 344 rats. Am. J. Physiol 274, R196–R203. [PubMed: 9458918]

Gemmell RT, Bell AW, and Alexander G (1972). Morphology of adipose cells in lambs at birth and during subsequent transition of brown to white adipose tissue in cold and in warm conditons. Am. J. Anat 133, 143–164. [PubMed: 5009244]

Geng Y, Dong Y, Yu M, Zhang L, Yan X, Sun J, Qiao L, Geng H, Nakajima M, Furuichi T, et al. (2011). Follistatin-like 1 (Fstl1) is a bone morphogenetic protein (BMP) 4 signaling antagonist in controlling mouse lung development. Proc. Natl. Acad. Sci. U S A 108, 7058–7063. [PubMed: 21482757]

Goncalves LF, Machado TQ, Castro-Pinheiro C, de Souza NG, Oliveira KJ, and Fernandes-Santos C (2017). Ageing is associated with brown adipose tissue remodelling and loss of white fat browning in female C57BL/6 mice. Int. J. Exp. Pathol 98, 100–108.

Graja A, Gohlke S, and Schulz TJ (2019). Aging of Brown and beige/brite adipose tissue. Handb. Exp. Pharmacol 251, 55–72. [PubMed: 30141100]

Hanssen MJ, Hoeks J, Brans B, van der Lans AA, Schaart G, van den Driessche JJ, Jorgensen JA, Boekschoten MV, Hesselink MK, Havekes B, et al. (2015). Short-term cold acclimation improves insulin sensitivity in patients with type 2 diabetes mellitus. Nat. Med 21, 863–865. [PubMed: 26147760]

Harms MJ, Ishibashi J, Wang W, Lim HW, Goyama S, Sato T, Kurokawa M, Won KJ, and Seale P (2014). Prdm16 is required for the maintenance of brown adipocyte identity and function in adult mice. Cell Metab. 19, 593–604. [PubMed: 24703692]

Heaton JM (1972). The distribution of brown adipose tissue in the human. J. Anat 112, 35–39. [PubMed: 5086212]

Horan MA, Little RA, Rothwell NJ, and Stock MJ (1988). Changes in body composition, brown adipose tissue activity and thermogenic capacity in BN/BiRij rats undergoing senescence. Exp. Gerontol 23, 455–461. [PubMed: 3250882]

Huttlin EL, Bruckner RJ, Paulo JA, Cannon JR, Ting L, Baltier K, Colby G, Gebreab F, Gygi MP, Parzen H, et al. (2017). Architecture of the human interactome defines protein communities and disease networks. Nature 545, 505–509. [PubMed: 28514442]

Jiang Y, Berry DC, and Graff JM (2017). Distinct cellular and molecular mechanisms for beta3 adrenergic receptor-induced beige adipocyte formation. Elife 6, e30329. [PubMed: 29019320]

Kang S, Bajnok L, Longo KA, Petersen RK, Hansen JB, Kristiansen K, and MacDougald OA (2005). Effects of Wnt signaling on brown adipocyte differentiation and metabolism mediated by PGC-1alpha. Mol. Cell Biol 25, 1272–1282. [PubMed: 15684380]

Kutyavin VI, and Chawla A (2019). BCL6 regulates brown adipocyte dormancy to maintain thermogenic reserve and fitness. Proc. Natl. Acad. Sci. U S A 116, 17071–17080. [PubMed: 31375635]

Lee YH, Petkova AP, Konkar AA, and Granneman JG (2015). Cellular origins of cold-induced brown adipocytes in adult mice. FASEB J. 29, 286–299. [PubMed: 25392270]

Li M, Li L, Li B, Hambly C, Wang G, Wu Y, Jin Z, Wang A, Niu C, Wolfrum C, et al. (2021). Brown adipose tissue is the key depot for glucose clearance in microbiota depleted mice. Nat. Commun 12, 4725. [PubMed: 34354051]

Lidell ME (2019). Brown adipose tissue in human infants. Handb. Exp. Pharmacol 251, 107–123. [PubMed: 29675580]

Liu X, Liu Y, Yang Z, and Ning W (2018). Cell type specific expression of Follistatin-like 1 (Fstl1) in mouse embryonic lung development. J. Mol. Histol 49, 399–409. [PubMed: 29916090]

Lo KA, Ng PY, Kabiri Z, Virshup D, and Sun L (2016). Wnt inhibition enhances browning of mouse primary white adipocytes. Adipocyte 5, 224–231. [PubMed: 27386162]

Loncar D (1991). Development of thermogenic adipose tissue. Int. J. Dev. Biol 35, 321–333. [PubMed: 1814413]

Mattiotti A, Prakash S, Barnett P, and van den Hoff MJB (2018). Follistatin-like 1 in development and human diseases. Cell Mol. Life Sci 75, 2339–2354. [PubMed: 29594389]

Maurer SF, Fromme T, Mocek S, Zimmermann A, and Klingenspor M (2019). Uncoupling protein 1 and the capacity for non-shivering thermogenesis are components of the glucose homeostatic system. Am. J. Physiol. Endocrinol. Metab 318, E198–E215. [PubMed: 31714796]

McDonald RB, Horwitz BA, Hamilton JS, and Stern JS (1988). Cold- and norepinephrine-induced thermogenesis in younger and older Fischer 344 rats. Am. J. Physiol 254, R457–R462. [PubMed: 3348440]

Merklin RJ (1974). Growth and distribution of human fetal brown fat. Anat. Rec 178, 637–645. [PubMed: 4856126]

Min SY, Kady J, Nam M, Rojas-Rodriguez R, Berkenwald A, Kim JH, Noh HL, Kim JK, Cooper MP, Fitzgibbons T, et al. (2016). Human 'brite/beige' adipocytes develop from capillary networks, and their implantation improves metabolic homeostasis in mice. Nat. Med 22, 312–318. [PubMed: 26808348]

Miyabe M, Ohashi K, Shibata R, Uemura Y, Ogura Y, Yuasa D, Kambara T, Kataoka Y, Yamamoto T, Matsuo K, et al. (2014). Muscle-derived follistatin-like 1 functions to reduce neointimal formation after vascular injury. Cardiovasc. Res 103, 111–120. [PubMed: 24743592]

Moser C, Straub LG, Rachamin Y, Dapito DH, Kulenkampff E, Ding L, Sun W, Modica S, Balaz M, and Wolfrum C (2021). Quantification of adipocyte numbers following adipose tissue remodeling. Cell Rep. 35, 109023. [PubMed: 33909996]

Niehrs C (2012). The complex world of WNT receptor signalling. Nat. Rev. Mol. Cell Biol 13, 767–779. [PubMed: 23151663]

Oelkrug R, Polymeropoulos ET, and Jastroch M (2015). Brown adipose tissue: physiological function and evolutionary significance. J. Comp. Physiol. B 785, 587–606.

Paul C, Sardet C, and Fabbrizio E (2015). The Wnt-target gene Dlk-1 is regulated by the Prmt5-associated factor Copr5 during adipogenic conversion. Biol. Open 4, 312–316. [PubMed: 25681392]

Prestwich TC, and Macdougald OA (2007). Wnt/beta-catenin signaling in adipogenesis and metabolism. Curr. Opin. Cell Biol 19, 612–617. [PubMed: 17997088]

Prieto-Echague V, Lodh S, Colman L, Bobba N, Santos L, Katsanis N, Escande C, Zaghloul NA, and Badano JL (2017). BBS4 regulates the expression and secretion of FSTL1, a protein that participates in ciliogenesis and the differentiation of 3T3-L1. Sci. Rep 7, 9765. [PubMed: 28852127]

Razzoli M, Frontini A, Gurney A, Mondini E, Cubuk C, Katz LS, Cero C, Bolan PJ, Dopazo J, Vidal-Puig A, et al. (2016). Stress-induced activation of brown adipose tissue prevents obesity in conditions of low adaptive thermogenesis. Mol. Metab 5, 19–33. [PubMed: 26844204]

Rogers NH (2015). Brown adipose tissue during puberty and with aging. Ann. Med 47, 142–149. [PubMed: 24888388]

Roh HC, Tsai LTY, Shao M, Tenen D, Shen Y, Kumari M, Lyubetskaya A, Jacobs C, Dawes B, Gupta RK, et al. (2018). Warming induces significant reprogramming of beige, but not Brown, adipocyte cellular identity. Cell Metab. 27, 1121–1137.e5. [PubMed: 29657031]

Rondini EA, and Granneman JG (2020). Single cell approaches to address adipose tissue stromal cell heterogeneity. Biochem. J 477, 583–600. [PubMed: 32026949]

Rosen ED, and Spiegelman BM (2014). What we talk about when we talk about fat. Cell 156, 20–44. [PubMed: 24439368]

Ruan HB (2020). Developmental and functional heterogeneity of thermogenic adipose tissue. J. Mol. Cell Biol 12, 775–784. [PubMed: 32569352]

Ruan HB, Dietrich MO, Liu ZW, Zimmer MR, Li MD, Singh JP, Zhang K,Yin R, Wu J, Horvath TL, et al. (2014). O-GlcNAc transferase enables AgRP neurons to suppress browning of white fat. Cell 159, 306–317. [PubMed: 25303527]

Ruan HB, Han X, Li MD, Singh JP, Qian K, Azarhoush S, Zhao L, Bennett AM, Samuel VT, Wu J, et al. (2012). O-GlcNAc transferase/host cell factor C1 complex regulates gluconeogenesis by modulating PGC-1α stability. Cell Metabolism 16, 226–237. [PubMed: 22883232]

Saito M, Okamatsu-Ogura Y, Matsushita M, Watanabe K, Yoneshiro T, Nio-Kobayashi J, Iwanaga T, Miyagawa M, Kameya T, Nakada K, et al. (2009). High incidence of metabolically active brown adipose tissue in healthy adult humans: effects of cold exposure and adiposity. Diabetes 58, 1526–1531. [PubMed: 19401428]

Sakaguchi M, Fujisaka S, Cai W, Winnay JN, Konishi M, O'Neill BT, Li M, Garcia-Martin R, Takahashi H, Hu J, et al. (2017). Adipocyte dynamics and reversible metabolic syndrome in mice with an inducible adipocyte-specific deletion of the insulin receptor. Cell Metab. 25, 448–462. [PubMed: 28065828]

Sanchez-Gurmaches J, and Guertin DA (2014). Adipocytes arise from multiple lineages that are heterogeneously and dynamically distributed. Nat. Commun 5, 4099. [PubMed: 24942009]

Sanchez-Gurmaches J, Hung CM, and Guertin DA (2016). Emerging complexities in adipocyte origins and identity. Trends Cell Biol. 26, 313–326. [PubMed: 26874575]

Schwalie PC, Dong H, Zachara M, Russeil J, Alpern D, Akchiche N, Caprara C, Sun W, Schlaudraff KU, Soldati G, et al. (2018). A stromal cell population that inhibits adipogenesis in mammalian fat depots. Nature 559, 103–108. [PubMed: 29925944]

Sellayah D, and Sikder D (2014). Orexin restores aging-related brown adipose tissue dysfunction in male mice. Endocrinology 155, 485–501. [PubMed: 24248466]

Shamsi F, Piper M, Ho LL, Huang TL, Gupta A, Streets A, Lynes MD, and Tseng YH (2021). Vascular smooth muscle-derived Trpv1(+) progenitors are a source of cold-induced thermogenic adipocytes. Nat. Metab 3, 485–495. [PubMed: 33846638]

Shapira SN, Lim HW, Rajakumari S, Sakers AP, Ishibashi J, Harms MJ, Won KJ, and Seale P (2017). EBF2 transcriptionally regulates brown adipogenesis via the histone reader DPF3 and the BAF chromatin remodeling complex. Genes Dev. 31, 660–673. [PubMed: 28428261]

Sidossis L, and Kajimura S (2015). Brown and beige fat in humans: thermogenic adipocytes that control energy and glucose homeostasis. J. Clin. Invest 125, 478–486. [PubMed: 25642708]

Stuart T, Butler A, Hoffman P, Hafemeister C, Papalexi E, Mauck WM 3rd, Hao Y, Stoeckius M, Smibert P, and Satija R (2019). Comprehensive integration of single-cell data. Cell 177, 1888–1902.e21. [PubMed: 31178118]

Sun W, Dong H, Balaz M, Slyper M, Drokhlyansky E, Colleluori G, Giordano A, Kovanicova Z, Stefanicka P, Balazova L, et al. (2020). snRNA-seq reveals a subpopulation of adipocytes that regulates thermogenesis. Nature 587, 98–102. [PubMed: 33116305]

Tabula Muris Consortium; Overall Coordination; Logistical Coordination; Organ Collection and Processing; Library Preparation and Sequencing; Computational Data Analysis; Cell Type Annotation; Writing Group; Supplemental Text Writing GROUP; Principal Investigators (2018). Single-cell transcriptomics of 20 mouse organs creates a Tabula Muris. Nature 562, 367–372. [PubMed: 30283141]

Tajima K, Ikeda K, Chang HY, Chang CH, Yoneshiro T, Oguri Y, Jun H, Wu J, Ishihama Y, and Kajimura S (2019). Mitochondrial lipoylation integrates age-associated decline in brown fat thermogenesis. Nat. Metab 1, 886–898. [PubMed: 32313871]

Tang QQ, and Lane MD (2012). Adipogenesis: from stem cell to adipocyte. Annu. Rev. Biochem 81, 715–736. [PubMed: 22463691]

Tanuma Y, Tamamoto M, Ito T, and Yokochi C (1975). The occurrence of brown adipose tissue in perirenal fat in Japanese. Arch. Histol. Jpn 38, 43–70. [PubMed: 1200786]

Timmons JA, Wennmalm K, Larsson O, Walden TB, Lassmann T, Petrovic N, Hamilton DL, Gimeno RE, Wahlestedt C, Baar K, et al. (2007). Myogenic gene expression signature establishes that brown and white adipocytes originate from distinct cell lineages. Proc. Natl. Acad. Sci. U S A 104, 4401–4406. [PubMed: 17360536]

van Marken Lichtenbelt WD, and Schrauwen P (2011). Implications of non-shivering thermogenesis for energy balance regulation in humans. Am. J. Physiol. Regul. Integr. Comp. Physiol 301, R285–R296. [PubMed: 21490370]

Wang CH, Lundh M, Fu A, Kriszt R, Huang TL, Lynes MD, Leiria LO, Shamsi F, Darcy J, Greenwood BP, et al. (2020). CRISPR-engineered human brown-like adipocytes prevent diet-induced obesity and ameliorate metabolic syndrome in mice. Sci. Transl. Med 12, eaaz8664. [PubMed: 32848096]

Wang W, Kissig M, Rajakumari S, Huang L, Lim HW, Won KJ, and Seale P (2014). Ebf2 is a selective marker of brown and beige adipogenic precursor cells. Proc. Natl. Acad. Sci. U S A 111, 14466–14471. [PubMed: 25197048]

Wang X, You L, Cui X, Li Y, Wang X, Xu P, Zhu L, Wen J, Pang L, Guo X, et al. (2018). Evaluation and optimization of differentiation conditions for human primary brown adipocytes. Sci. Rep 8, 5304. [PubMed: 29593245]

Wu Y, Zhou S, and Smas CM (2010). Downregulated expression of the secreted glycoprotein follistatin-like 1 (Fstl1) is a robust hallmark of preadipocyte to adipocyte conversion. Mech. Dev 127, 183–202. [PubMed: 20043993]

Xue R, Lynes MD, Dreyfuss JM, Shamsi F, Schulz TJ, Zhang H, Huang TL, Townsend KL, Li Y, Takahashi H, et al. (2015). Clonal analyses and gene profiling identify genetic biomarkers of the thermogenic potential of human brown and white preadipocytes. Nat. Med 21, 760–768. [PubMed: 26076036]

Yang X, and Ruan HB (2015). Neuronal control of adaptive thermogenesis. Front. Endocrinol. (Lausanne) 6, 149. [PubMed: 26441839]

Ye Y, Liu H, Zhang F, and Hu F (2019). mTOR signaling in Brown and Beige adipocytes: implications for thermogenesis and obesity. Nutr. Metab. (Lond) 16, 74. [PubMed: 31708995]

Yoneshiro T, Aita S, Matsushita M, Okamatsu-Ogura Y, Kameya T, Kawai Y, Miyagawa M, Tsujisaki M, and Saito M (2011). Age-related decrease in cold-activated brown adipose tissue and accumulation of body fat in healthy humans. Obesity (Silver Spring) 19, 1755–1760. [PubMed: 21566561]

Yoneshiro T, Wang Q, Tajima K, Matsushita M, Maki H, Igarashi K, Dai Z, White PJ, McGarrah RW, Ilkayeva OR, et al. (2019). BCAA catabolism in brown fat controls energy homeostasis through SLC25A44. Nature 572, 614–619. [PubMed: 31435015]

Zeng X, Ye M, Resch JM, Jedrychowski MP, Hu B, Lowell BB, Ginty DD, and Spiegelman BM (2019). Innervation of thermogenic adipose tissue via a calsyntenin 3beta-S100b axis. Nature 569, 229–235. [PubMed: 31043739]

Zoico E, Rubele S, De Caro A, Nori N, Mazzali G, Fantin F, Rossi A, and Zamboni M (2019). Brown and beige adipose tissue and aging. Front. Endocrinol. (Lausanne) 10, 368. [PubMed: 31281288]

Highlights

- Rabbit BAT involutes in a manner similar to human
- Analogous progenitor hierarchy exists in human and rabbit BAT
- BAT involution is associated with restricted adipogenic capacity of FSTL1^{+} progenitors
- Deleting the *Fstl1* gene or *Fstl1*$^{+}$ progenitors leads to BAT paucity in mice

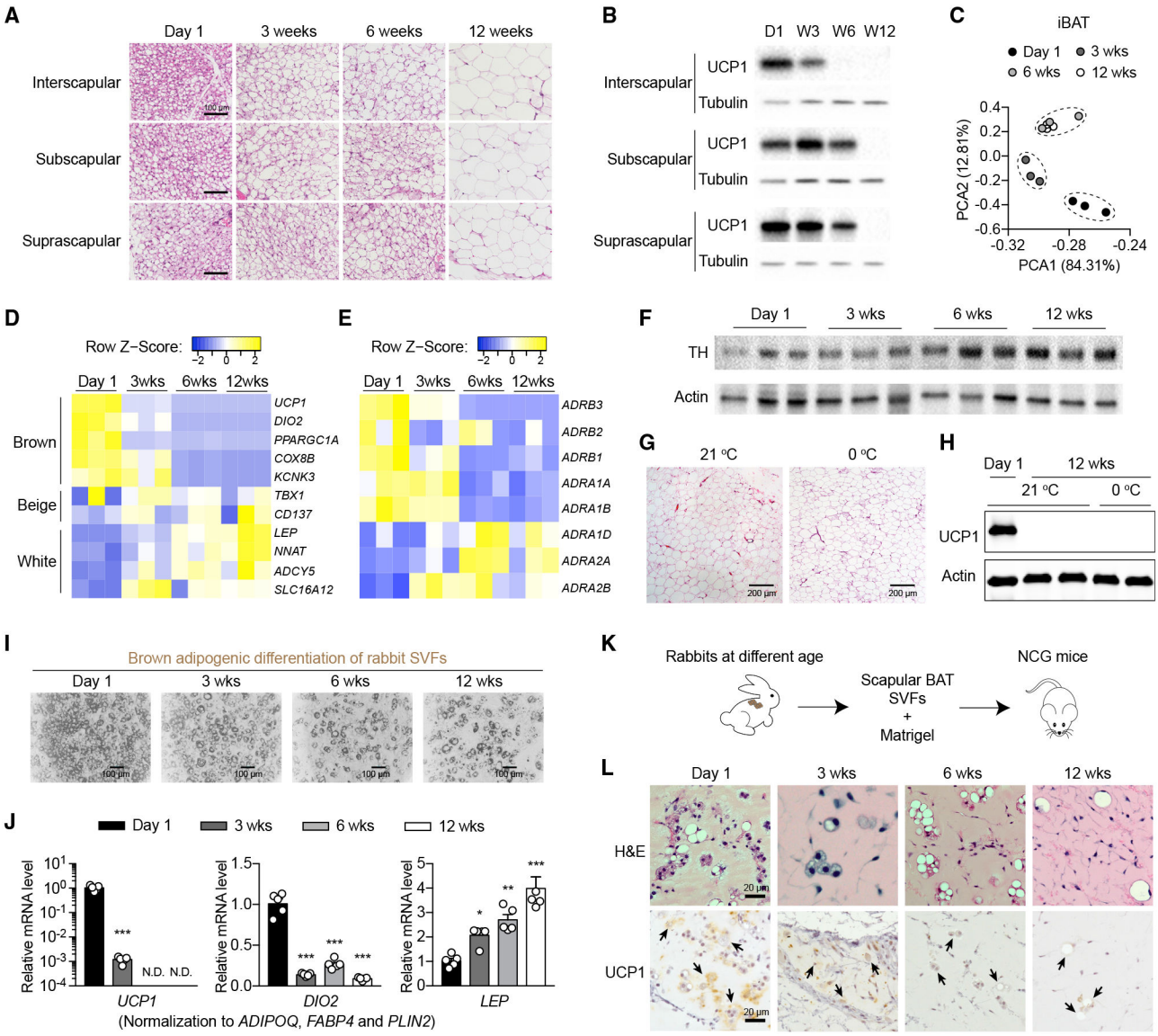

Figure 1. Histological and transcriptional remodeling of rabbit BAT

(A and B) Representative H&E images (A) and UCP1 protein expression (B) of BAT depots from rabbits at different ages (n = 3). Scale bars represent 100 μm.

(C) Principal-component analysis (PCA) plot of rabbit iBAT at different ages after RNA-seq.

(D and E) Expression heatmaps of adipocyte marker genes (D) and AR genes (E). Coloring indicates fragments per kilobase million (FPKM) values (high, yellow; low, blue).

(F) Expression of TH protein in iBAT of rabbits at the indicated ages.

(G and H) Representative H&E images (G) and UCP1 protein expression (H) of iBAT depots from adult rabbits collected at summer or early spring (n = 2).

(I and J) Rabbit iBAT SVF cells were differentiated using a brown adipogenic cocktail.

(I) Lipid deposition in differentiated cells.

(J) Relative gene expression normalized to geometric mean of *ADIPOQ, FABP4*, and *PLIN2* (n = 5).

(K and L) Rabbit SVF cells from periscapular BAT were implanted into NCG mice (K, n = 3). Representative H&E and UCP1 immunohistochemistry of implants are shown in (L). Arrows indicate adipocytes.

*p < 0.05, **p < 0.01, ***p < 0.001 by one-way ANOVA followed by Tukey's multiple comparisons.

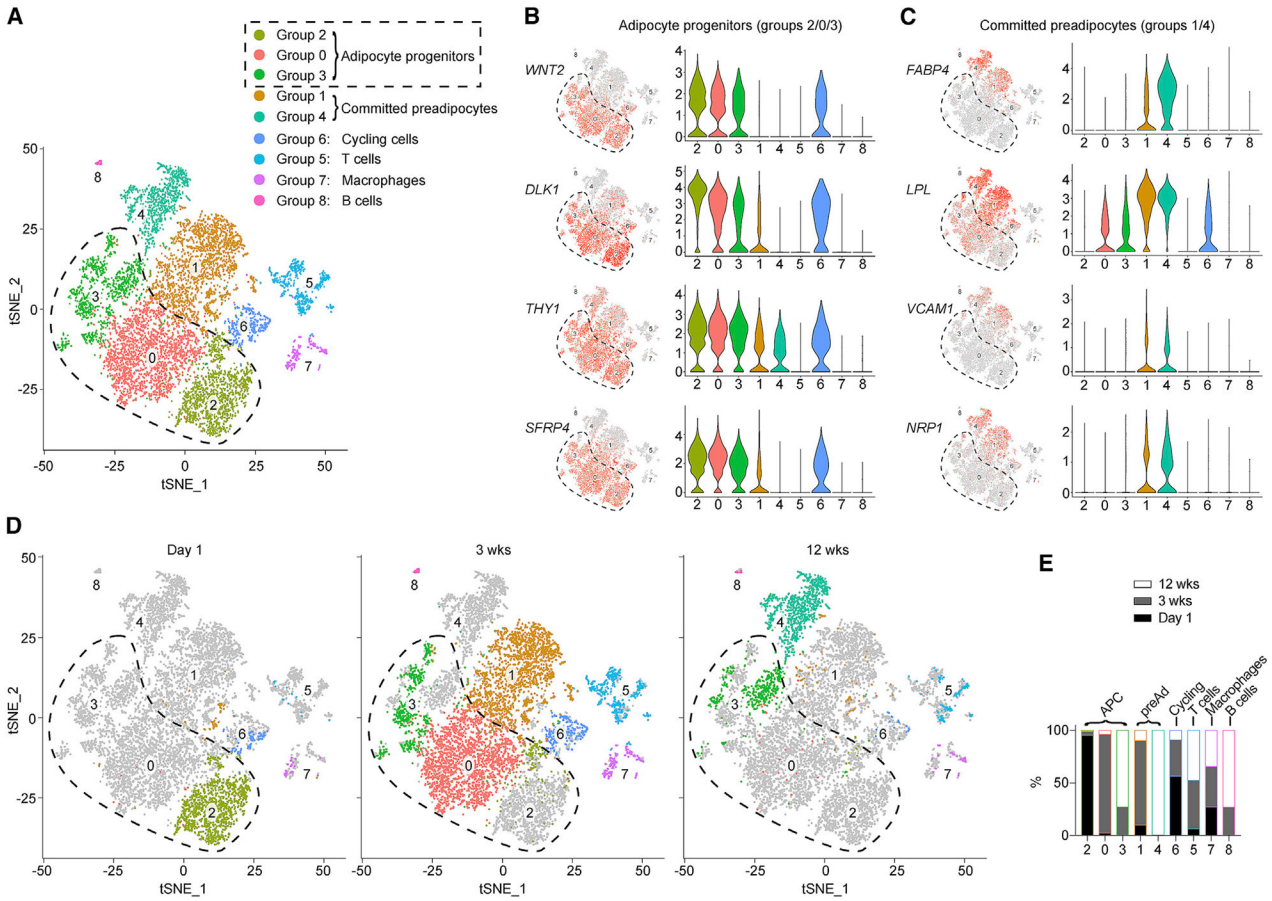

Figure 2. Transcriptional dynamics of rabbit iBAT SVF cells at the single-cell level

(A) t-distributed stochastic neighbor embedding (tSNE) plot showing 9 distinct groups of cells clustered from pooled iBAT SVFs of 1-day-, 3-week-, and 12-week-old rabbits.

(B and C) tSNE and violin plots showing the expression levels and distribution of marker genes for adipocyte progenitors (B) and committed preadipocytes (C).

(D) tSNE plot of iBAT SVF cells segregated by age.

(E) Distribution of different-aged SVF cells within each cell group.

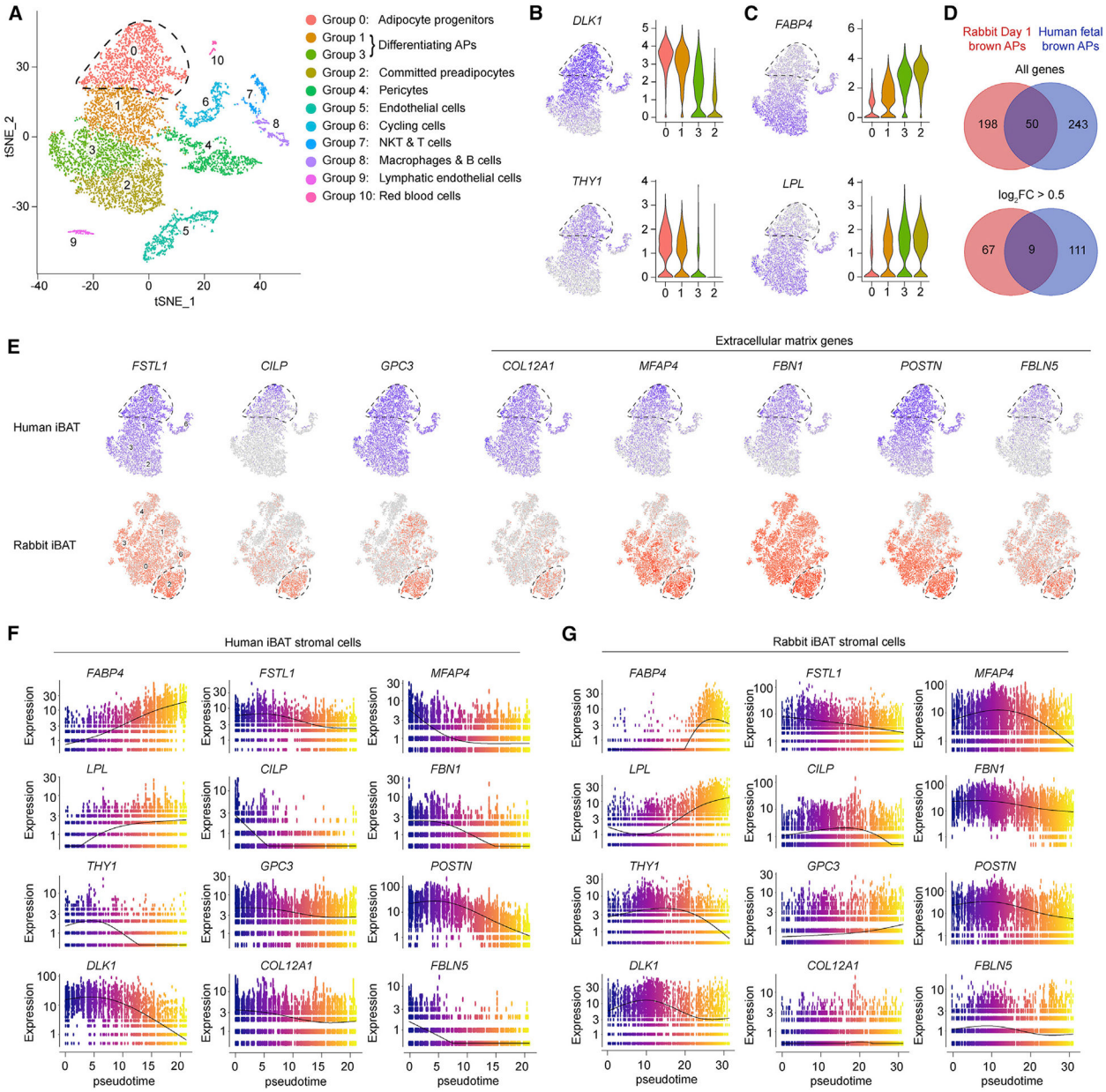

Figure 3. Analogy between human and rabbit brown adipocyte progenitors

(A) tSNE plot showing 11 clustered groups of SVF cells from human fetal iBAT.

(B and C) tSNE and violin plots showing the expression levels and distribution of marker genes for brown adipocyte progenitors (B) and committed brown preadipocytes (C).

(D) Venn diagrams of numbers of common mark genes between rabbit group 2 and human group 0 progenitors. Top: all marker genes. Bottom: marker genes with log2 fold change > 0.5.

(E) tSNE plots showing the distribution of common marker genes for brown adipocyte progenitors between human (top) and rabbit (bottom).

(F and G) Expression dynamics of feature genes in human (F) and rabbit (G) iBAT stromal cells as a function of pseudotime.

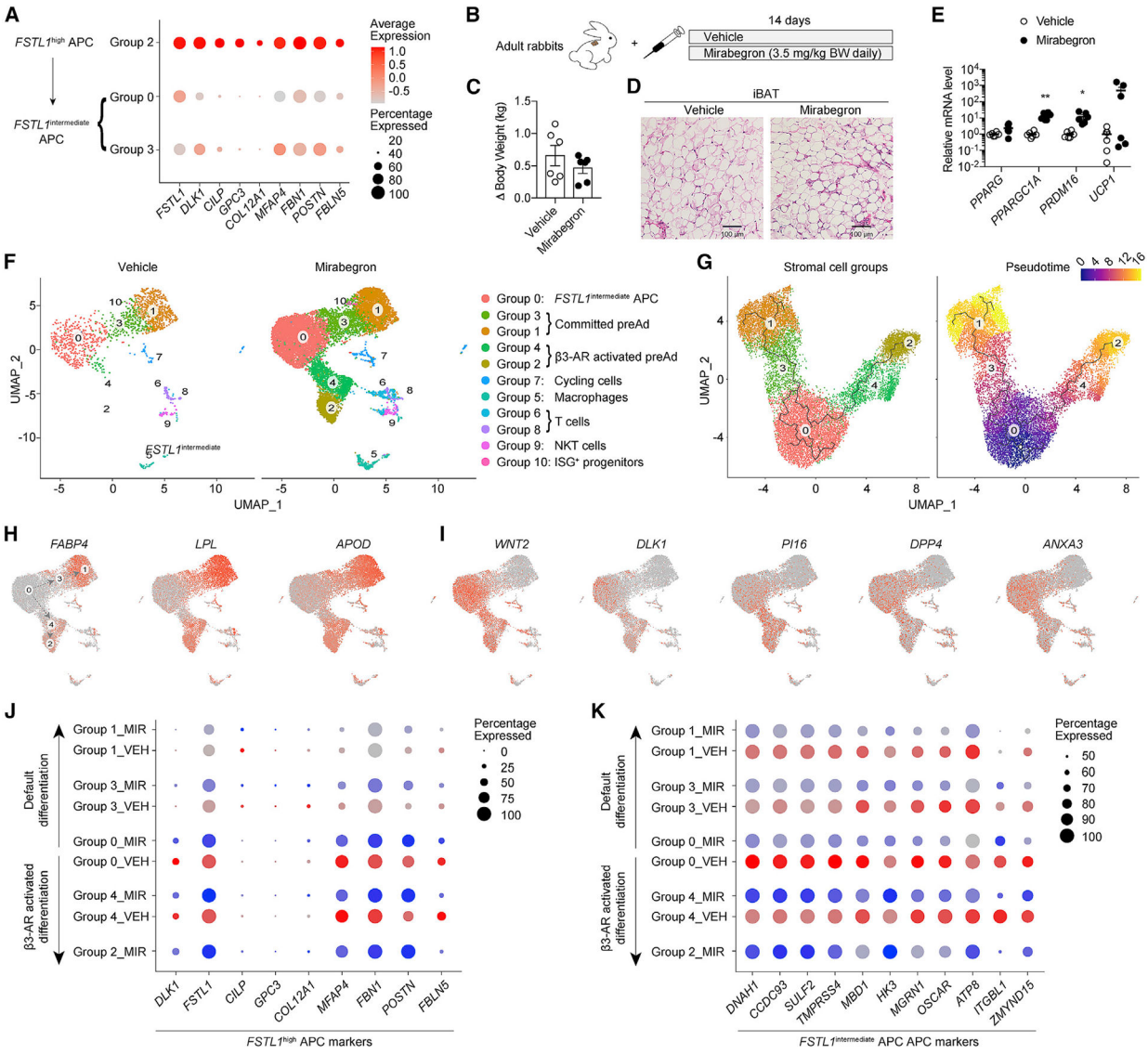

Figure 4. Adipocyte progenitors from involuted rabbit iBAT are refractory to β3-AR induction

(A) Dot plot showing the average expression of 9 common APC markers and their percentages expressed in *FSTL1*^{high} versus *FSTL1*^{intermediate} SVF cells.

(B–E) 12-week-old rabbits were injected daily with vehicle or mirabegron (n = 6, two independent experiments) for 2 weeks (B). Changes in body weight (C), morphology of iBAT (D), and thermogenic gene expression in iBAT (E) were determined.

(F) Uniform manifold approximation and projection (UMAP) plots showing 11 integrated clusters of SVF cells from vehicle- and mirabegron-treated adult rabbits. ISG, interferon-stimulated gene.

(G) Cell trajectory (left) and pseudotime analysis (right) of rabbit SVF stromal cells, computed by Monocle3.

(H and I) UMAP plots showing the expression distribution of adipocyte feature genes (H) and white adipocyte progenitor marks (I).

(J and K) Dot plots showing the expression level (color intensity) and percentage (circle size) of *FSTL1*^{high} brown APC markers (J) and *FSTL1*^{intermediate} white APC markers (K) in SVF stromal cells before (red) and after (blue) mirabegron treatment.

Data are presented as mean ± SEM (C and E). *$p < 0.05$, **$p < 0.01$ by unpaired Student's t test.

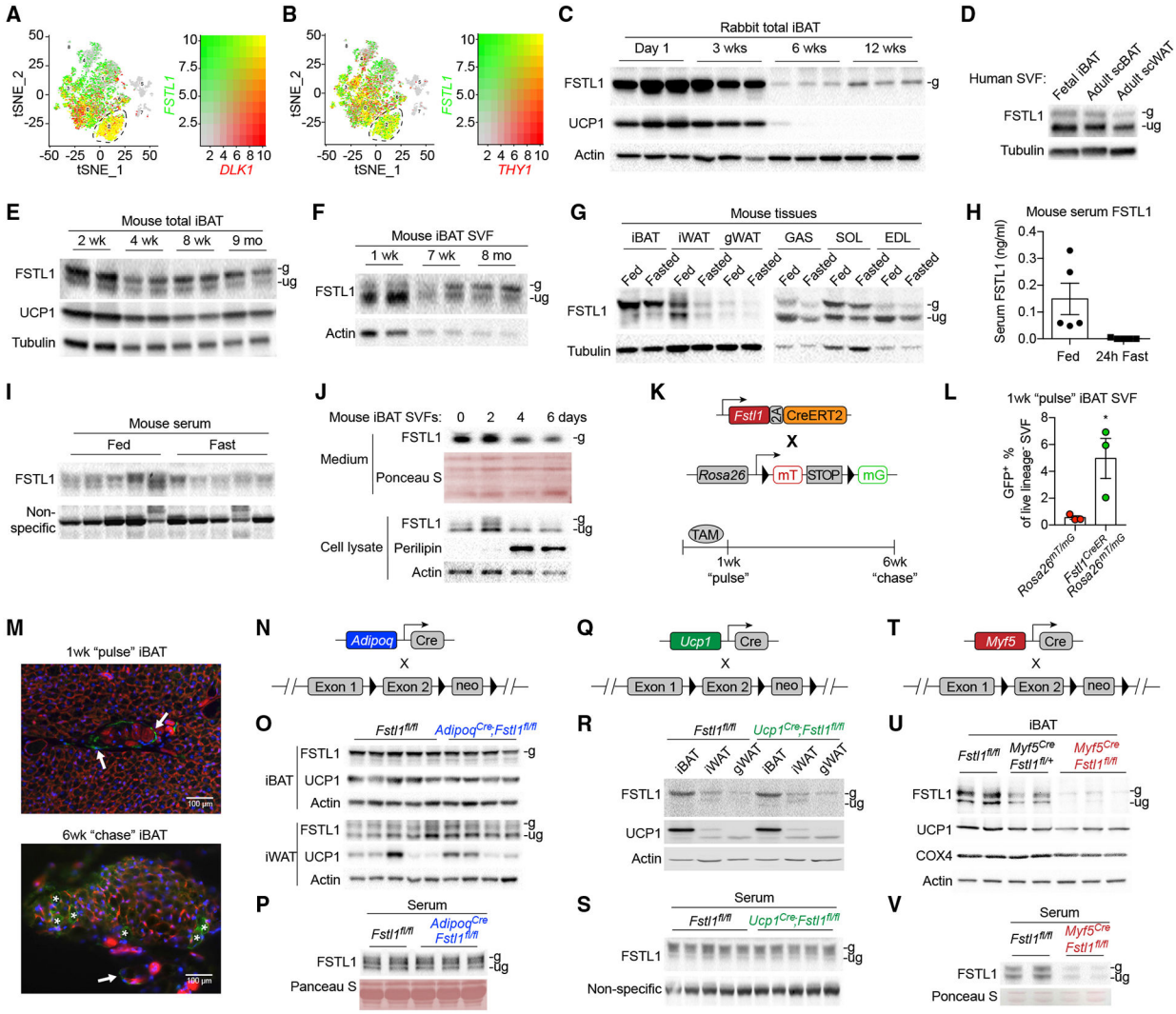

Figure 5. FSTL1 is a brown adipocyte progenitor-enriched factor

(A and B) tSNE plots showing co-expression of *FSTL1* with *DLK1* (A) and *THY1* (B) in rabbit iBAT SVF cells.

(C) Expression of FSTL1 and UCP1 protein in total iBAT from rabbits at the indicated ages. "g" and "ug" indicate glycosylated and unglycosylated FSTL1, respectively.

(D) FSTL1 protein expression in SVF cells from human fetal iBAT, adult suprascapular (sc)BAT, and adult scWAT.

(E) FSTL1 and UCP1 protein expression in iBAT from female mice at the indicated ages.

(F) FSTL1 protein expression in iBAT SVF cells from mice at the indicated ages.

(G) FSTL1 protein expression in iBAT, iWAT, and gWAT and *gastrocnemius* (GAS), *soleus* (SOL), and *extensor digitorum longus* (EDL) muscle from mice fed ad libitum or fasted for 24 h.

(H and I) FSTL1 levels in the serum of mice fed *ad libitum* or fasted for 24 h (n = 5), determined by ELISA (H) and western blot (I).

(J) FSTL1 protein expression and secretion into medium during adipogenic differentiation of mouse iBAT SVF cells.

(K–M) 4-week-old *Fstl1*^{CreERT2};*Rosa26*$^{mT/mG}$ mice were pulsed and chased (K). GFP^{+} cells as percentage of total live lineage^{-} SVF cells were quantified by flow cytometry (L). Perivascular GFP^{+} cells at pulse (arrows) and differentiated brown adipocytes at chase (asterisks) were imaged (M).

(N–P) Generation of adipocyte-specific FSTL1 KO (N). FSTL1 and UCP1 protein expression in iBAT and WAT depots (O) and serum FSTL1 levels (P) of adult mice was determined.

(Q–S) Generation of brown/beige adipocyte-specific FSTL1 KO (Q). FSTL1 and UCP1 protein expression in iBAT and WAT depots (R) and serum FSTL1 levels (S) of adult mice was determined.

(T–V) Deletion of the *Fstl1* gene in the *Myf5* lineage (T). Protein expression in iBAT (U) and serum FSTL1 levels (V) of neonatal mice were determined.

Data are presented as mean ± SEM. *$p < 0.05$ by unpaired Student's t test.

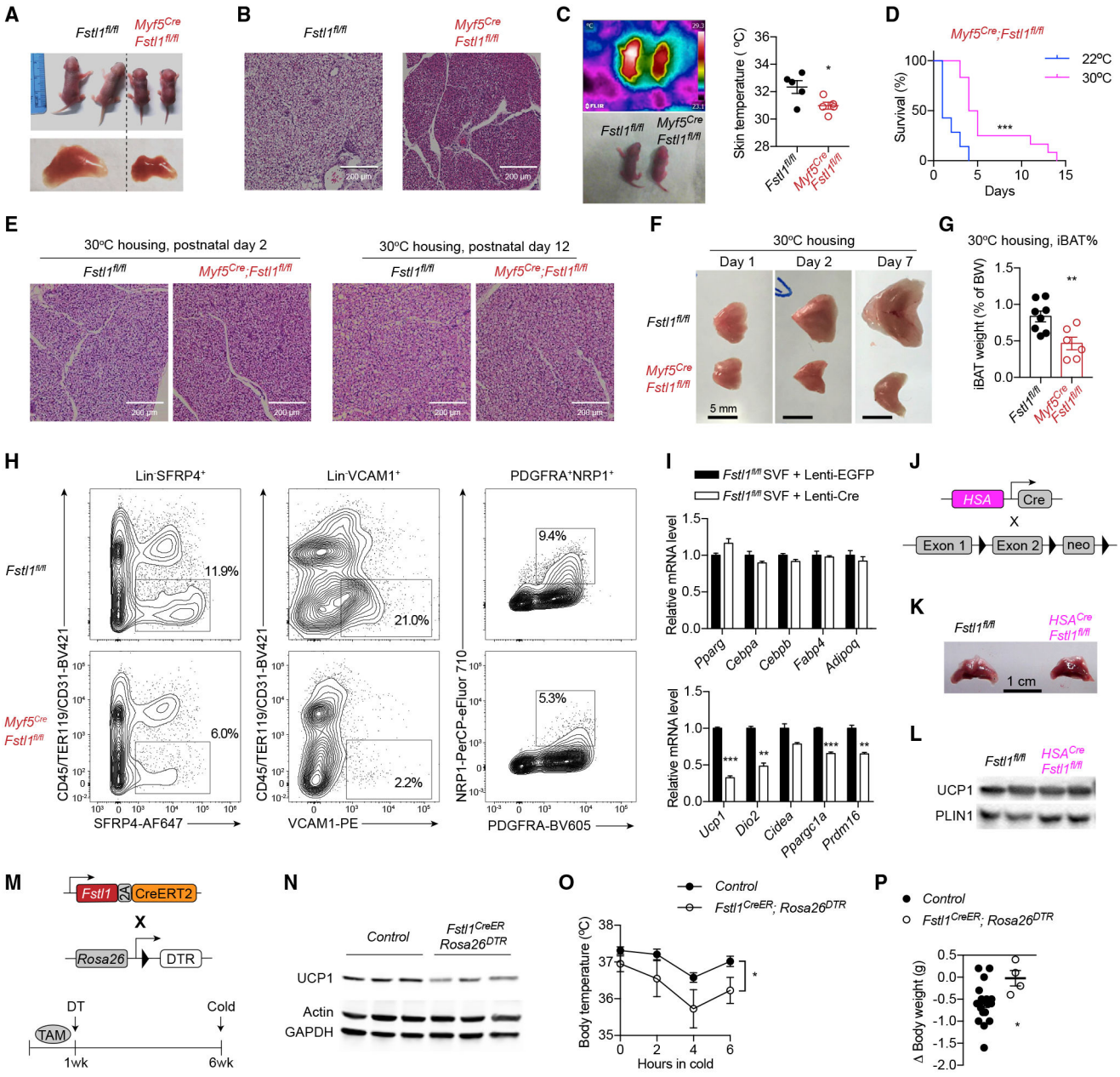

Figure 6. iBAT paucity in *Myf5^{Cre};Fstl1$^{fl/fl}$* mice

(A) 3-day-old control and *Myf5^{Cre};Fstl1$^{fl/fl}$* KO mice housed at room temperature (RT) and the size of iBAT.

(B) Histology of iBAT of 3-day-old mice housed at RT.

(C) Body surface temperature of newborn mice separated from dams at RT for 3 h. Periscapular skin temperature is quantified on the right (n = 5).

(D) Survival curves of *Myf5^{Cre};Fstl1$^{fl/fl}$* KO mice housed at 22°C (n = 8) or 30°C (n = 12).

(E) Histology of iBAT from 2- and 12-day-old mice housed at 30°C.

(F) Morphology of iBAT from mice housed at 30°C.

(G) iBAT-to-body weight ratio of 4- to 5-day-old female mice housed at 30°C (n = 6–8).

(H) Flow cytometry quantification of adipocyte progenitors ($Lin^{-}SFRP4^{+}$) and committed preadipocytes ($Lin^{-}SFRP4^{+}$ and $Lin^{-}PDGFRA^{+}NRP1^{+}$) within the SVF of iBAT from 7-day-old mice housed at RT.

(I) *Fstl1*$^{fl/fl}$ iBAT SVF cells were infected with lentiviruses expressing EGFP or Cre recombinase, followed by adipogenic differentiation. Expression of genes involved in adipogenesis and thermogenesis was determined (n = 3).

(J–L) Generation of skeletal muscle-specific FSTL1 KO (J). iBAT morphology (K) and UCP1 protein expression (L) from adult mice were determined.

(M–P) *Fstl1*^{CreERT2};*Rosa26*^{DTR} mice were generated for DT-mediated cell ablation (M). Shown is expression of UCP1 protein in iBAT (N). Rectal temperature was determined during acute cold challenge (O). Body weight loss upon 6-h cold treatment was measured (P).

Data are presented as mean ± SEM. *p < 0.05, **p < 0.01, ***p < 0.001 by unpaired Student's t test (C, G, I, and P), two-way ANOVA (O), and Mantel-Cox test (D).

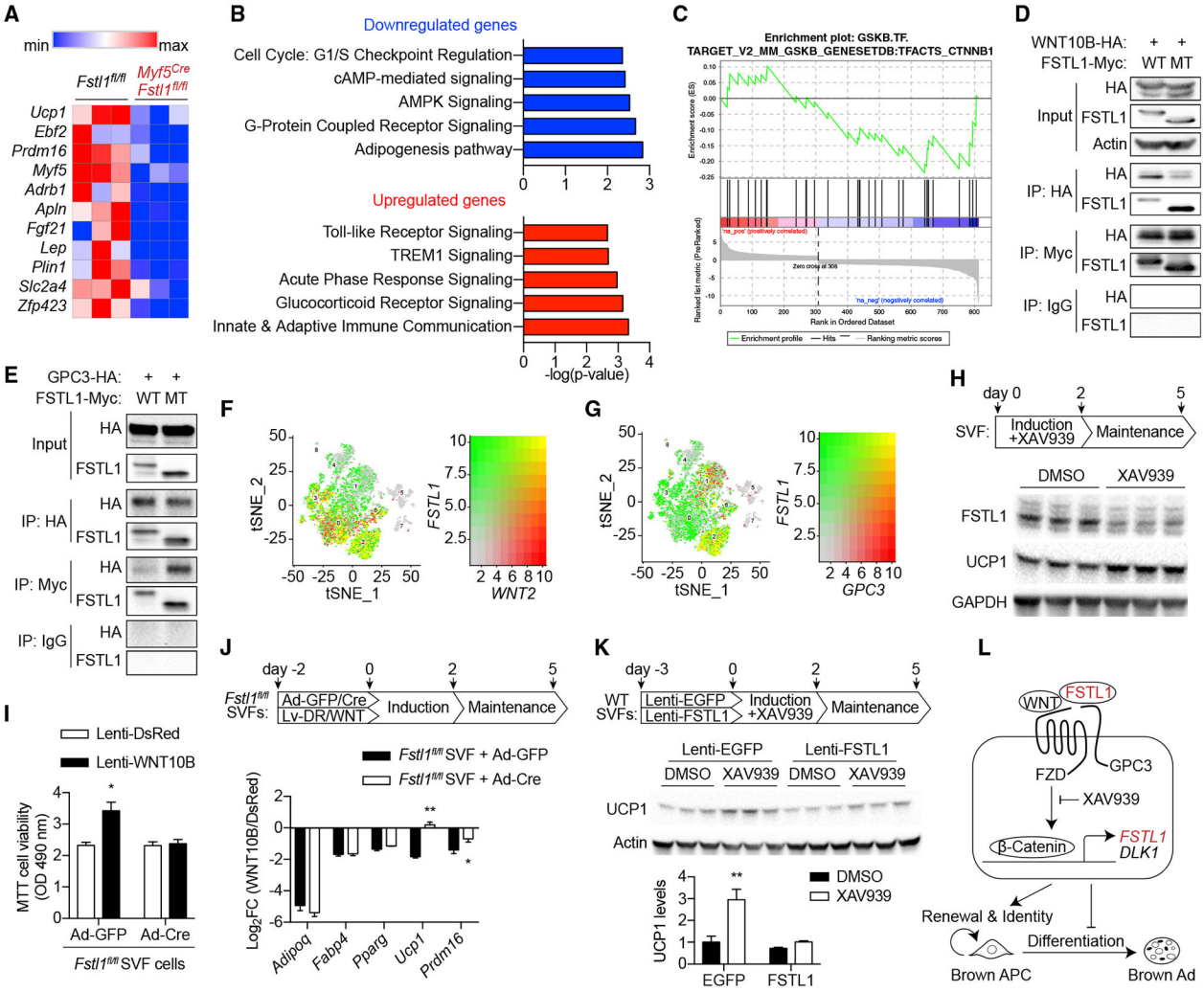

Figure 7. FSTL1 cooperates with WNT signaling in iBAT development

(A) Expression heatmap of selected markers of thermogenesis and adipogenesis.

(B) Ingenuity pathway analysis (IPA) of pathways enriched in downregulated (top) and upregulated (bottom) genes in *Myf5*^{Cre};*Fstl1*$^{fl/fl}$ KO iBAT.

(C) Enrichment plots for β-catenin-regulated genes from the gene set enrichment analysis (GSEA).

(D and E) Interaction of wild-type (WT) and glycosylation-mutant (MT; N142/173/178Q) FSTL1 with WNT10B (D) or GPC3 (E) in HEK293 cells.

(F and G) tSNE plots showing co-expression of *FSTL1* with *WNT2* (F) and *GPC3* (G) in rabbit iBAT SVF cells.

(H) iBAT SVF cells were differentiated in the absence or presence of XAV939. FSTL1 and UCP1 were blotted.

(I and J) *Fstl1*$^{fl/fl}$ iBAT SVF cells were infected with a Cre adenovirus to induce *Fstl1* gene deletion. WNT10B was overexpressed via lentiviral vectors. A 3-(4,5-dimethylthiazol-2-yl)-2,5-diphenyltetrazolium bromide (MTT) proliferation assay of undifferentiated cells at 72 h (I, n = 5) and qRT-PCR of adipogenic and thermogenic genes of differentiated cells (J, n = 6) were performed.

(K) iBAT SVF cells were infected with lentiviral vectors expressing GFP or FSTL1, followed by treatment with DMSO or XAV939 during adipogenic induction. UCP1 protein was blotted and quantified.

(L) Schematic of the FSTL1-WNT interplay in brown adipocyte progenitor renewal and identity maintenance.

Data are presented as mean ± SEM. *$p < 0.05$, **$p < 0.01$ by two-way ANOVA (I and K) and unpaired Student's t test (J).

KEY RESOURCES TABLE

REAGENT or RESOURCE	SOURCE	IDENTIFIER
Antibodies		
Anti-UCP1 (Dilution 1:5000 WB& 1:5000 IHC)	Abcam	Cat# ab209483; RRID:AB_2722676
Anti-UCP1 (Dilution1:500 IF for Human sample)	Sigma	Cat# U6382; RRID:AB_261838
Anti-Tubulin (Dilution 1:2000 WB)	Proteintech	Cat# 66031-1-1g; RRID:AB_11042766
Anti-FSTL1 (Dilution 1:500 WB)	R&D Systems	Cat# AF1738; RRID:AB_354962
Anti-Actin (Dilution 1:5000 WB)	Sigma-Aldrich	Cat# 5441; RRID:AB_476744
Anti-Perilipin (Dilution 1:1000 WB)	Cell Signaling Technology	Cat# 9349; RRID:AB_10829911
Anti-GAPDH (Dilution 1:2000 WB)	Bioworld	Cat# MB001; RRID:AB_2857326
Anti-COX4 (Dilution 1:1000 WB)	Proteintech	Cat# 11242-1-AP; RRID:AB_2085278
Anti-β-Catenin (Dilution 1:1000 WB)	Cell Signaling Technology	Cat# 8480; RRID:AB_11127855
Anti-HA (2 μg IP)	Proteintech	Cat# 51064-2-AP; RRID:AB_11042321
Anti-HA (Dilution 1:1000 WB)	Roche	Cat# 11583816001; RRID:AB_514505
Anti-Myc (2 μg IP)	Proteintech	Cat# 16286-1-AP; RRID:AB_11182162
Anti-TH (Dilution 1:1000 WB)	Cell Signaling Technology	Cat# 13106; RRID:AB_2798122
Anti-CD31 (Dilution 1:100 IF)	Bioworld	Cat# BS1574; RRID:AB_1663692
Anti-Cleaved Caspase-3	Cell Signaling Technology	Cat# 9661S; RRID:AB_2341188
Anti-CD45-BV421 (Dilution 1:100 FACS)	BD Bioscience	Cat# 564279; RRID:AB_2651134
Anti-TER119-BV421 (Dilution 1:100 FACS)	BioLegend	Cat# 116234; AB_2562917
Anti-CD31-BV421 (Dilution 1:100 FACS)	BioLegend	Cat# 102424; RRID:AB_2650892
Anti-SFRP4 (Dilution 1:100 FACS)	Abcam	Cat# ab154167
Anti-VCAM1-PE (Dilution 1:100 FACS)	BioLegend	Cat# 105713; RRID:AB_1134164
Anti-NRP1-PerCP-eFluor710 (Dilution 1:100 FACS)	Thermo Fisher Scientific	Cat# 46-3041-80; RRID:AB_2573740
Anti-PDGFRA-BV605 (Dilution 1:100 FACS)	BioLegend	Cat# 135916; RRID:AB_2721548
Anti-Mouse IgG-HRP (Dilution 1:10000 WB)	Cell Signaling Technology	Cat# 7076; RRID:AB_330924
Anti-Rabbit IgG-HRP (Dilution 1:10000 WB)	Cell Signaling Technology	Cat# 7074; RRID:AB_2099233
Anti-Goat IgG-HRP (Dilution 1:10000 WB)	Santa Cruz Biotechnology	Cat# SC2020; RRID:AB_631728
Anti-Rabbit IgG-AF647 (Dilution 1:200 FACS)	BioLegend	Cat# 406414; AB_2563202
Anti-Rabbit IgG-AF488 (Dilution 1:1000 IF)	Thermo Fisher Scientific	Cat# R37118; RRID:AB_2556546
Anti-Rabbit IgG-Dylight 488 (Dilution 1:1000 IF for human sample)	Bioworld	Cat# BS10017
Normal Rabbit IgG (2 μg IP)	Santa Cruz Biotechnology	Cat# SC-2027; RRID:AB_737197
Bacterial and virus strains		
Adenovirus-EGFP	Ruan et al., 2012	N/A
Adenovirus-Cre	Ruan et al., 2012	N/A
Chemicals, peptides, and recombinant proteins		
DMEM	Corning	Cat#10-017-CV
DMEM/F12	Corning	Cat#10-090-CV
Adipocyte Medium	Sciencell	Cat#7201
FBS	GenClone	Cat#25-514
PBS	Corning	Cat#20-040-CV
HBSS	Thermo Fisher Scientific	Cat#14175-095

REAGENT or RESOURCE	SOURCE	IDENTIFIER
HEPAS	Thermo Fisher Scientific	Cat#15630-080
Penicillin-Streptomycin (Pen-Strep)	Thermo Fisher Scientific	Cat#15140122
70um Filter	Fisher Brand	Cat#22363548
Collagenase I (for mouse and rabbit samples)	Worthington	Cat#LS004196
Collagenase I (for human sample)	Diomond	Cat#A004194
Liver Digest Medium	Thermo Fisher Scientific	Cat# 17703-034
40um Filter	Fisher Brand	Cat#22363549
ACK Buffer (for mouse and rabbit sample)	Quality Biological	Cat#118-156-101
ACK Buffer (For human sample)	Sangon Biotech	Cat#B541001
Ciprofloxacin HCl	Sigma-Aldrich	Cat#PHR1044
Blasticidin	InvivoGen	Cat#ant-bl
Primocin	InvivoGen	Cat#ant-pm-1
MTT (3-(4,5-Dimethylthiazol-2-yl)-2,5-Diphenyltetrazolium Bromide)	Sigma-Aldrich	Cat#M2128
PEI Max	Polysciences	Cat# 24765-1
Insulin (Novolin R®)	Novo Nordisk	Cat# 0169-1833-11
T3 (3,3′,5-Triiodo-L-thyronine sodium salt)	Sigma-Aldrich	Cat#T6397
IBMX (3-Isobutyl-1-methylxanthine)	Sigma-Aldrich	Cat#I5879
Rosiglitazone	Sigma-Aldrich	Cat#R2408
Dexamethasone	Sigma-Aldrich	Cat#D4902
Indomethacin	Sigma-Aldrich	Cat#I7378
Biotin	Sigma-Aldrich	Cat# B4639
Transferrin	Sigma-Aldrich	Cat# T8158
D-Pantothenic Acid	RPI	Cat#P55650
Primocin	InvivoGen	Cat#ant-pm-1
2-Deoxy-D-Glucose (2-DG)	Sigma-Aldrich	Cat#D6134
Mirabegron	XA BC-Biotech	N/A
CL316,243	Tocris	Cat#1499
Basal DMEM	Sigma-Aldrich	Cat#D5030
GlutaMax™	Thermo Fisher Scientific	Cat#13462629
Fatty acid-free BAS	Sigma-Aldrich	Cat#A3803
Oligomycin	Sigma-Aldrich	Cat#O4876
Antimycin	Sigma-Aldrich	Cat#A8674
Norepinephrine	Sigma-Aldrich	Cat#A9512
TRIzol	Thermo Fisher Scientific	Cat# 15596026
Matrigel	Coring	Cat#356237
Isoflurane	Piramal	Cat#66704-013-025
DMSO	Sigma-Aldrich	Cat#D4540
KolliphorEL	Sigma-Aldrich	Cat#C5135
Protein A/G	Santa Cruz Biotechnology	Cat#SC-2027
Formalin solution	Sigma-Aldrich	Cat#HT501128
VECTASHIELD® Antifade Mounting Medium with DAPI	Vector	Cat#H-1200

REAGENT or RESOURCE	SOURCE	IDENTIFIER
Target Retrieval Solution, Citrate pH 6.1	Agilent	Cat#S1699
Critical commercial assays		
Dead cell removal kit	Miltenyi Biotec	Cat#130-090-101
Fixable Viability Dye eFluor™ 780	eBioscience	65-0865-14
PureLink™ RNA Mini Kit	Thermo Fisher Scientific	Cat#12183018A
iScript™ cDNA Synthesis Kit	Bio-Rad	Cat#1708891
iTaq™ Universal SYBR® Green Supermix	Bio-Rad	Cat#172-5125
Histostain®-Plus 3rd Gen IHC Detection Kit	Thermo Fisher Scientific	Cat#85-9073
Deposited data		
RNA-seq of iBAT from Myf5-Fslt1 KO mice	This paper	GSE148888
Bluk and scRNA-seq of rabbit BAT	This paper	GSE148891
Experimental models: Cell lines		
hTERT A41hBAT-SVF	ATCC	CRL-3385
hTERT A41hWAT-SVF	ATCC	CRL-3386
Human fetal BAT SVF	Xue et al., 2015	N/A
Mouse iBAT SVF	This paper	N/A
Rabbit iBAT SVF	This paper	N/A
293FT	Thermo Fisher Scientific	Cat#R70007
Experimental models: Organisms/strains		
Fstl1$^{fl/fl}$: B6-Fstl1$^{f3,4/+}$/Nju	National Resource Center for Mutant Mice of China	Stock No: B000172
Ucp1-Cre: B6.FVB-Tg(Ucp1-cre)1Evdr/J	The Jackson Laboratory	Stock No: 024670
Myf5-Cre: B6.129S4-Myf5$^{tm3(cre)Sor}$/J	The Jackson Laboratory	Stock No: 007893
Adipoq-Cre: B6;FVB-Tg(Adipoq-cre)1Evdr/J	The Jackson Laboratory	Stock No: 010803
HSA-Cre: B6.Cg-Tg(ACTA1-cre)79Jme/J	The Jackson Laboratory	Stock No: 006149
Fstl1-CreER: B6N;129-Fstl1$^{tm1(CreERT2)}$/Nju	National Resource Center for Mutant Mice of China	N/A
Rosa26-mTmG: B6.129(Cg)-Gt(ROSA)26Sortm4(ACTB-tdTomato,-EGFP)Luo/J	The Jackson Laboratory	Stock No: 007676
Rosa26-DTR:C57BL/6-Gt(ROSA)26Sortm1(HBEGF)Awai/J	The Jackson Laboratory	Stock No: 007900
NCG: NOD-Prkdc^{em26Cd52}Il2rg^{em26Cd22}/NjuCrl	Charles River	572
New Zealand White Rabbits	Bakkom Rabbitry	N/A
Oligonucleotides		
Table S11	This paper	N/A
Recombinant DNA		
Plasmid: pLenti-SV40T-P2a-Blasticidin	This paper	N/A
Plasmid: pLXSN2-Wnt10b-HA (NM_011718.2)	Kang et al., 2005	N/A
Plasmid: pLVX-FSTL1-Myc WT(NM_008047.5)	This paper	N/A
Plasmid: pLVX-FSTL1-MycMT(N142Q;N173Q;N178Q)	This paper	N/A
Plasmid: pSPAX2	Addgene	#12260
Plasmid: pMD2G	Addgene	#12259
Plasmid: pLVX-Dsred-MonoN1	Clontech	Cat#632152

REAGENT or RESOURCE	SOURCE	IDENTIFIER
Plasmid: pLVX-Wnt10b (NM_011718.2)	This paper	N/A
Software and algorithms		
FLIR Tools	5.13	https://www.flir.com/products/flir-tools/
Excel	v16.16.21	https://www.microsoft.com
Graphpad	v7.0	https://www.graphpad.com
FlowJo	v10	https://www.flowjo.com
SOAPnuke	v1.5.2	https://github.com/BGI-flexlab/SOAPnuke
HISAT2	v2.0.4	http://daehwankimlab.github.io/hisat2/
Bowtie2	v2.2.5	http://bowtie-bio.sourceforge.net/bowtie2
RSEM	V1.2.12	http://deweylab.biostat.wisc.edu/RSEM
DEseq2	V1.26.0	https://bioconductor.org/packages/release/bioc/html/DESeq2.html
Cell Ranger Single Cell Software Suite	v3.1.0	https://www.10xgenomics.com
Seurat	v3.1.5	https://satijalab.org/seurat/